Lithos 390–391 (2021) 106115

Contents lists available at ScienceDirect

Lithos

journal homepage: www.elsevier.com/locate/lithos

Research Article

Genesis and age of Pb—Zn mineralization from the Ningi-Burra ring complex, North Central Nigeria: Constraints from zircon morphology, U—Pb dating and Lu—Hf isotopes

Victor Ikechukwu Vincent [a,b,c], Huan Li [b,*], Musa Bala Girei [b,c,d], Hafizullah Abba Ahmed [e], Eyo Eyo Ntekim [e]

[a] School of Earth Sciences, China University of Geosciences, Wuhan 430074, China
[b] Key Laboratory of Metallogenic Prediction of Nonferrous Metals and Geological Environment Monitoring, Ministry of Education, School of Geosciences and Info-Physics, Central South University, Changsha 410083, China
[c] Department of Resources Science and Engineering, School of Earth Resources, China University of Geosciences, Wuhan 430074, China
[d] Department of Geology, Faculty of Earth and Environmental Sciences, Bayero University Kano, Kano State, Nigeria
[e] Department of Geology, Modibbo Adama University of Technology, P.M.B. 2076 Yola, Nigeria

ARTICLE INFO

Article history:
Received 14 December 2020
Received in revised form 26 February 2021
Accepted 6 March 2021
Available online 16 March 2021

Keywords:
Hydrothermally-altered zircon
Zircon trace element
U–Pb isotope
Lu-Hf isotope
Ningi-Burra

ABSTRACT

The Ningi-Burra Pb—Zn mineralization forms part of the Nigerian Sn-Nb ± (Pb-Zn-Mo)-rich anorogenic alkaline province, also known as the Nigerian Younger Granite Complexes. Six distinct *E*-W trending magmatic centres have been identified in the Ningi-Burra complex, but the Pb—Zn mineralization is confined to highly evolved biotite granite in Koluki (centre 6). In this paper, a combination of geochronological and geochemical data of magmatic and hydrothermally-altered zircon from the Ningi-Burra complex are used to constrain magmatic and hydrothermal processes that facilitated the formation of Pb—Zn mineralization. Zircon trace element and Hf isotopes ($\varepsilon Hf(t) = -5.3$ to -10.3) indicate that the parental magma of these ore-bearing granites were largely derived from lower crustal sources with contributions from the upper mantle. The hydrothermal alteration that accompanied the Pb—Zn mineralization include silicification, chloritization and limited sodic metasomatism. Zircon U/Pb dating reveal that magma emplacement and subsequent hydrothermal process in Ningi-Burra complex occurred at (~192 Ma) and (<191 Ma), respectively. Zircon grains from unmineralized and hydrothermally altered rock suites have similar $^{176}Hf/^{177}Hf$ but distinct $^{176}Lu/^{177}Hf$ and $^{176}Yb/^{177}Hf$ ratios which suggest a magmatic source for the hydrothermal fluids responsible for the formation of the mineralization. This study highlights the application of zircon trace element and U-Th-Hf isotopes as robust tools for constraining magmatic and mineralization process that facilitate the formation of economically significant mineralization in highly differentiated granites.

1. Introduction

Zircon, a ubiquitous accessory mineral in various rock types, has continued to generated a lot of research interest due to its chemical resilience and ability to record distinct geological events (Valley et al., 2010). Zircon trace element geochemistry, U/Pb dating and Lu/Hf isotopes are widely used in several aspects of petrological studies (Jiang et al., 2019a; Wang et al., 2019). Remarkably, zircon preserve unique internal structures, zonation and geochronological information (Hoskin and Schaltegger, 2003) which can be used to delineate complex geologic processes (e.g. metamorphism, granitic emplacement, and mineralization). These unique characteristics have led to the application of zircon as crucial indicators of sediment provenance (Belousova et al., 2002), magma crystallization temperature and evolutionary history (Grimes et al., 2009; Watson and Harrison, 2005). The increased viability of high-precision geochronological dating of zircon (Schoene et al., 2010) and the robust nature of Lu/Hf isotope systems in zircon (Kemp et al., 2007) permits constrains on timing and nature of magmatic events based on geochronological, geochemical and isotopic records in zircon. These distinct records are particularly useful in elucidating pertinent information about the origin and evolution of multi-phased granitic systems.

Varying temperature and chemical regimes during the evolution of highly fractionated F-rich granite may be accompanied by metamictization of magmatic zircons and/or crystallization of hydrothermal zircons. Although the term "hydrothermal zircon" was coined in the 1990s to denote zircon that exhibits geochemical and geochronological signatures distinct from those of magmatic zircon, it is still very difficult to distinguish typical hydrothermal zircon from metamorphic zircon (Hoskin, 2005; Nardi et al., 2013). Nonetheless, several parameters including crystal morphology (e.g. spongy textures with multiple

* Corresponding author.
E-mail address: lihuan@csu.edu.cn (H. Li).

https://doi.org/10.1016/j.lithos.2021.106115
0024-4937/

inclusions), internal texture, moderately high common Pb and distinct trace element patterns have been used to distinguish hydrothermal zircon from typical magmatic and metamorphic zircon (Hoskin, 2005; Hoskin and Schaltegger, 2003). Investigations of hydrothermal zircon in magmatic-hydrothermal systems have proved a reliable tool in investigating fluid-rock alteration mechanisms and timing of single/multi-staged magmatic-mineralization episodes (Li et al., 2014; Wang et al., 2019). Increased mobility of zirconium and other relatively "immobile" elements during hydrothermal alteration events in alkali and F-rich granitic systems allow for tracking of physicochemical conditions related to magmatic-hydrothermal evolution and its bearing on ore formation (Hoskin, 2005; Jiang et al., 2019a; Kebede et al., 2007; Li et al., 2014; Li et al., 2018; Rubin et al., 1993).

Mesozoic anorogenic ring complexes are distributed over an area of 160 km by 400 km and extend from Northern Nigeria to Central Nigeria. These anorogenic ring complexes are commonly referred to as the "Nigerian Younger Granites". The emplacement of these anorogenic granites in Nigeria was controlled by some deep-seated transcurrent fault systems and spanned a long period from late Triassic to early Cretaceous (216–141 Ma; Rahaman et al., 1984; Girei et al., 2019). These high-level alkaline intrusions are spatially associated with Sn-Nb ± (Pb-Zn-Mo) mineralization (Girei et al., 2019; Kinnaird, 1985). Recent geochemical and geophysical studies have advanced our understanding of these rare metal granites including the distribution of their associated mineralization (Girei et al., 2019). In addition, several geochemical studies have been carried out on ore-bearing granites in the Mesozoic anorogenic plutons of Nigeria (Kinnaird et al., 1985). However, these studies have focused primarily on Sn—W bearing lodes. Geochemical and isotopic of Pb—Zn bearing granites can provide new insights into the complex magmatic-hydrothermal processes that led to the formation of sulfide mineralization in these highly evolved Mesozoic granites.

In this study, we used a combination of zircon cathodoluminescence (CL), U/Pb age and Lu/Hf isotope data for barren granites, mineralized granites and ore-bearing veins to constrain the origin and timing of magmatic and hydrothermal processes that are associated with Pb—Zn mineralization in the Ningi-Burra complex.

2. Geology and petrology

2.1. Regional geology

The Nigerian Mesozoic anorogenic complexes cover an area 400 km and 160 km wide and intruded quartzofeldspatic Precambrian basement rocks (Fig. 1a-b). Structural and geochronological studies (Rahaman et al., 1984) have shown that the emplacement of the Mesozoic anorogenic ring complexes of Nigeria was primarily controlled by N-S trending shears and transcurrent faults (Fig. 1a). These shear zones and faults appear to have formed during the terminal stage of the Pan-African orogeny (Black et al., 1985). The basement complex rocks of Nigeria retain signatures of an Eburnian and Pan-African orogenic episode (Bute et al., 2019; Dickin et al., 1991). The Pan-African episode is the most intense and widespread orogenic event with localized

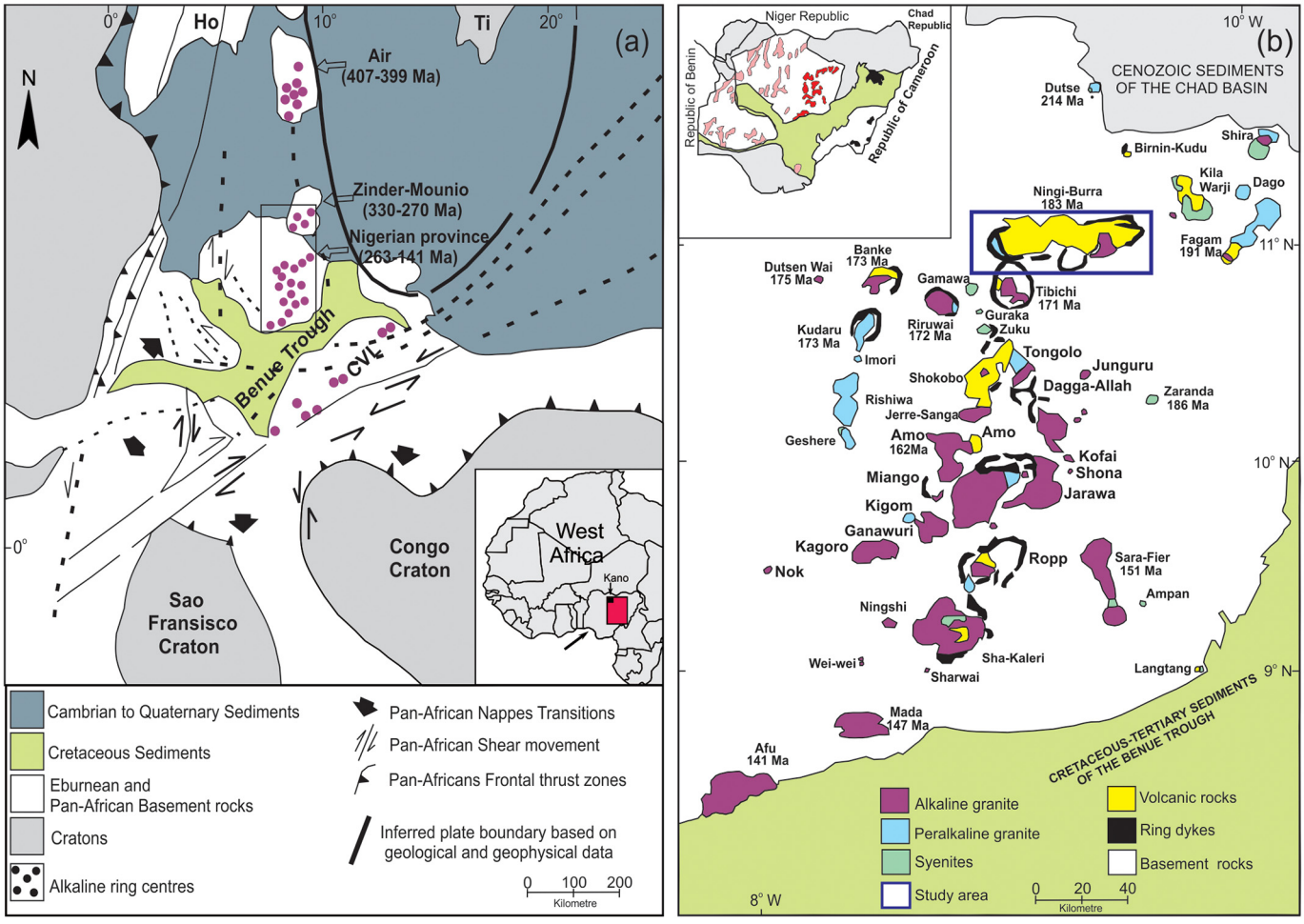

Fig. 1. Schematic map showing the distribution of anorogenic complexes in the (a) West African Craton and (b) Nigerian Younger Granite Field (Modified from Kinnaird, 1985). Rb—Sr Age Data taken from Rahaman et al. (1984) and Van Breemen et al. (1975).

isotopic homogenization of crustal terrains reported in Eastern Nigeria (Turner, 1983). In the Nigerian sector, the Pan-African episode primarily generated *syn*-collisional to post-collisional rocks of granitic, monzodioritic and charnokitic composition (Bute et al., 2019). Black et al. (1979) have suggested continent-continent collision of the West African Craton and with an active eastern continent during the closing stages of the Pan-African orogeny. In parts of western and eastern Nigeria, emplacement of alkaline magmatism took place shortly after the end of the Pan-African event (Black et al., 1985) signifying transitions from active orogenic episodes through post-collisional to within-plate settings. This transition cycle represents a classic example of evolutions associated with orogenic events worldwide (Black et al., 1985). However, the emplacement of the alkaline ring complexes of Niger-Nigeria province (480–141 Ma) began long after the end of the Pan African orogeny and signify a distinct phase of "within-plate" magmatism in the West African Craton (Black et al., 1985; Bowden and Kinnaird, 1984). According to Black et al. (1985), emplacement for the ring complex in the Northern Niger centres begin in the early Silurian (430–400 Ma), emplacement for the alkaline ring complexes in Southern Nigeria was significant during the Carboniferous (330–260 Ma), and emplacement in the Nigerian sector began in the Triassic and continued till the Early Cretaceous (214–141 Ma).

Extrusions of comendite, ignimbritic rhyolites and minor trachytes mark the first phase of igneous activities in the Nigerian ring complexes. Subsequent cauldron collapse and ring fracturing gave rise to ring dykes composed of granite/quartz porphyries (Ike, 1983). These ring dykes which are predominantly fayalite bearing represent the first phase of plutonic intrusions in the anorogenic complexes (Ike, 1983). Granitic intrusions then follow the emplacement of the granite/quartz porphyries. Magmatism in the Nigerian Younger granite complex are mostly acidic in composition with intermediate and basic rocks comprising about 5% of the complexes (Kinnaird, 1985). Peralkaline granites are confined to the southern anorogenic complexes, whereas aluminous biotite granites occur in both the northern and southern complexes and their emplacement marked the final stage of the anorogenic magmatism (Amuda et al., 2020). Locally, late-stage metasomatism and/or post-magmatic hydrothermal alterations intensely alter the granitic suites and are associated with Sn-W-Mo-W mineralization in biotite granites (Girei et al., 2020), Nb-REE mineralization in arfvedsonite granites (Ogunleye et al., 2006), Cu + (Py) mineralization in granite porphyries (Olatunji and Ekwere, 1986) and Sn-W-sulphide mineralization in adjoining basement rocks (Kinnaird, 1984). Principally, biotite granite suites within the anorogenic complexes of Nigeria have undergone the most intense alteration and roof zones of these biotite granite suites contain economically significant rare-metal mineralization (Kinnaird, 1984; Kinnaird et al., 1985). Primarily, mineralization styles in the biotite granite vary from disseminated, stockworks, altered wall rock to vein-type occurrences. However, the most developed vein systems associated with world-class Sn–Nb–W–Zn lodes are best expressed in the Ririwai, Tibchi, and Afu complexes (Kinnaird, 1985).

2.2. Geology of the Ningi-Burra Pb—Zn Ore field

The Ningi-Burra complex comprises six overlapping magmatic centres that trend in *E*-W direction and cover a total area of 1400 km^2 (Fig. 1b). Detail descriptions of the petrology and structural evolution of these distinct magmatic centres have been provided by Turner and Bowden (1979). The sequential magmatic activity in each centre started with volcanic eruption during which small volume of crystal-poor ignimbrites was emplaced. This was successively followed by ring fracturing, stopping and emplacement of syenites and co-genetic arfvedsonite granite and biotite granite (Turner and Bowden, 1979).

In the Koluki-Burra centre (centre 6), biotite granites host Pb-Zn-Cu and Sn-Nb-Ta mineralization (Fig. 2a). The biotite granite phase makes up the central part of the plutonic suites of the Koluki-Burra centre (Fig. 2b).

Two distinct sulphide deposits are found in the Koluki-Burra centre (Fig. 2a) namely: (i) the Jigawa Pb—Zn mineralization (this study) and (ii) the Limi Pb—Zn mineralization. Although mineralization in the Koluki-Burra centre is associated with the biotite granite suites, altered zones at the boundaries between biotite granite and arfvedsonite granites suites are associated with disseminated mineralization hosted in both granitic suites. The Jigawa Pb—Zn deposits are located in the Koluki-Burra centre (Centre 6) of the Ningi-Burra complex and consist of both disseminated and vein-type Pb—Zn mineralization (Fig. 2b). The mineralized veins range in size from several cm to 1 m in width and can be up to 100 m long. Local swarming of these veins has led to the development of workable lodes (Fig. 3a). Based on available field evidence, the major alteration phases associated with the Jigawa Pb—Zn deposit are chloritization, potassic metasomatism, and silicification. The peculiar reddening of the altered rocks (Fig. 3b, d) is related to the hematization and dissolution of magnetite during potassic metasomatism (Abaa, 1991). Deposition of quartz in cavities during silicification phases in the Jigawa Pb—Zn deposit is often accompanied by disseminated mineralization (Fig. 3b). This alteration phase predominantly presents as quartz with accompanied sphalerite and galena crystals (Fig. 3c). Moreover, this alteration style has been reported as crucial to the formation of the giant Ririwai Sn-Pb-Zn deposit (Kinnaird et al., 1985) and is also economically important for the introduction of sulphides in the Jigawa Pb—Zn deposit. Mineralized quartz veins presents as either milky or glassy quartz crystals perpendicular to the adjoining wall rock. Ore minerals associated with the Jigawa Pb—Zn mineralization includes galena, sphalerite and chalcopyrite. Malachite and hematite are formed as part of supergene alteration of the ore bodies.

3. Sampling and analytical methods

A total of seven samples, two from each of the unmineralized granites (KLK1A and CHR1), hydrothermally altered granites (AT1A and AT1B) and three from ore-bearing wall rock & quartz veins (JK1A, JK2A and JK6A) were collected from the Jigawa Pb—Zn deposit (Fig. 2b). The unmineralized biotite granites which occur as a set of high-level plutons (Fig. 3) show distinct variations in texture ranging from medium-grained pinkish types to coarse-grained white-pinkish types with large feldspar crystals (Fig. 4a). In thin section, they contain quartz (25%), K-feldspar (40%), and biotite (10%) with accessory magnetite, zircon and titanite. Sample KLK1A is a medium to coarse-grained biotite granite from centre 6 (Fig. 4c). Under the microscope, the matrix is primarily composed of K-feldspar (30%), quartz (20%), perthite (10%), and biotite (15%). Accessory minerals include zircon, titanite, apatite and magnetite. Oxidation of opaque minerals and biotite is apparent both in hand specimens and under the microscope (Fig. 4c-d). Altered granitic suites (Fig. 4g-l) associated with mineralization in the Jigawa Pb—Zn field show varying degrees and styles of alteration. Complete chloritization of biotite is evident in highly altered wall rocks (Fig. 4e), and reddened facies of the granites display substantial evidence for potassic metasomatism. The degree of alteration is higher in Sample AT1A, where only small patches retain relict textures of the original granite (Fig. 4f). The rock is porphyritic in texture. In thin sections, equigranular groundmass consists of K-feldspar (40%), quartz (35%), biotite (15%) and minor plagioclases and hornblende. Accessory minerals include zircon and titanite. Biotite and feldspar grains have been altered to chlorite and muscovite (Fig. 4e-f). Sample AT1B is medium- to coarse-grained, greyish to greenish, and display evidence of potassic alteration or hematization (Fig. 4g). In thin section, the essential minerals are quartz (30%), K-feldspar (45%), and biotite (15%), with zircon as an accessory mineral. Specks of galena and sphalerite are seen across altered fronts in photomicrographs (Fig. 4h).

Mineralized ore samples were collected from different section representative of styles of mineralization in the Jigawa Pb—Zn ore field. Sample JK1A was taken from a silicified wall rock sections in the western end of the ore vein where massive sphalerite crystals with specks of

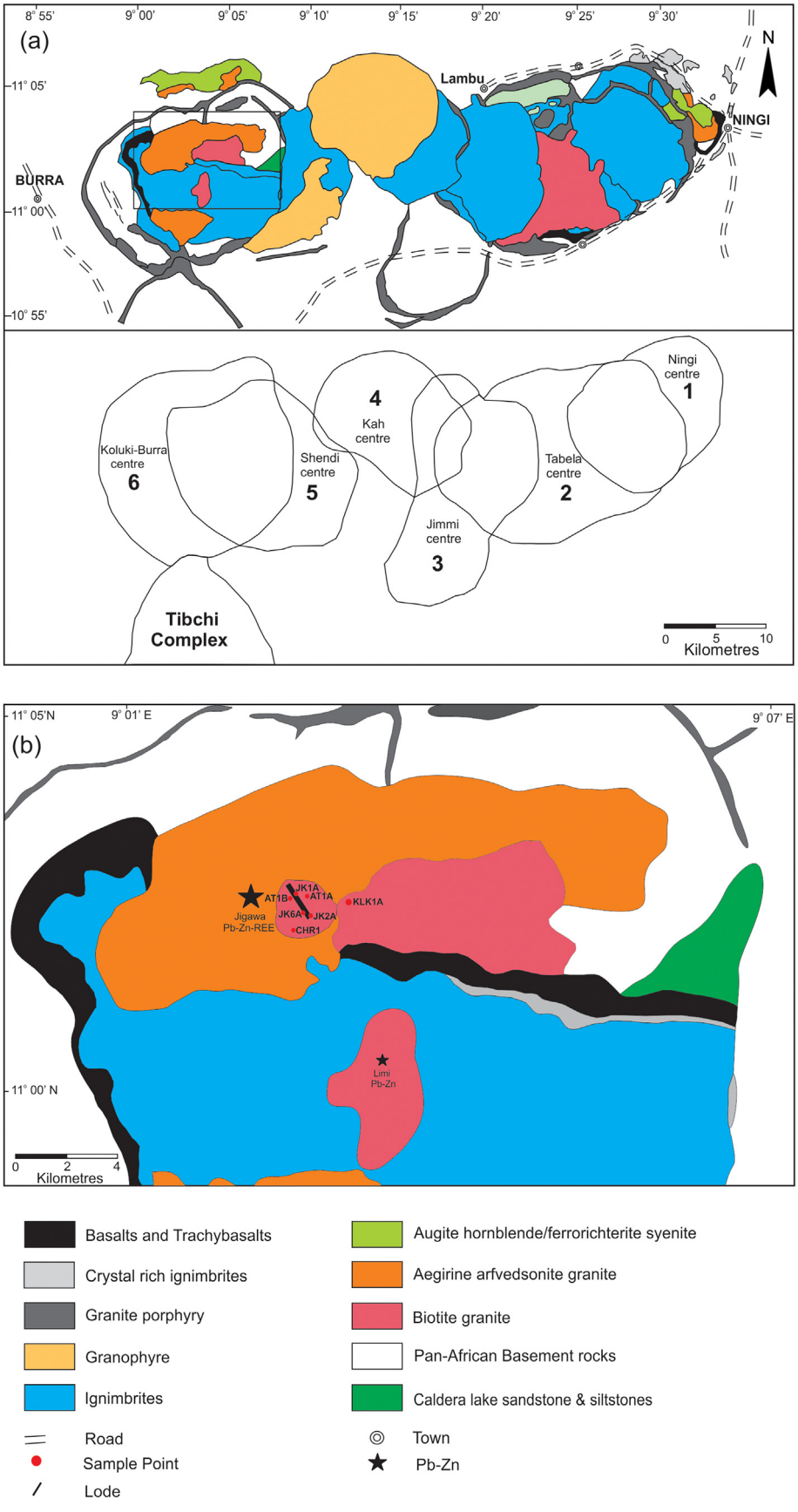

Fig. 2. Geologic Map of (a) the Ningi-Burra Complex and (b) of the Jigawa Pb–Zn ore field. Modified from Turner and Bowden (1979).

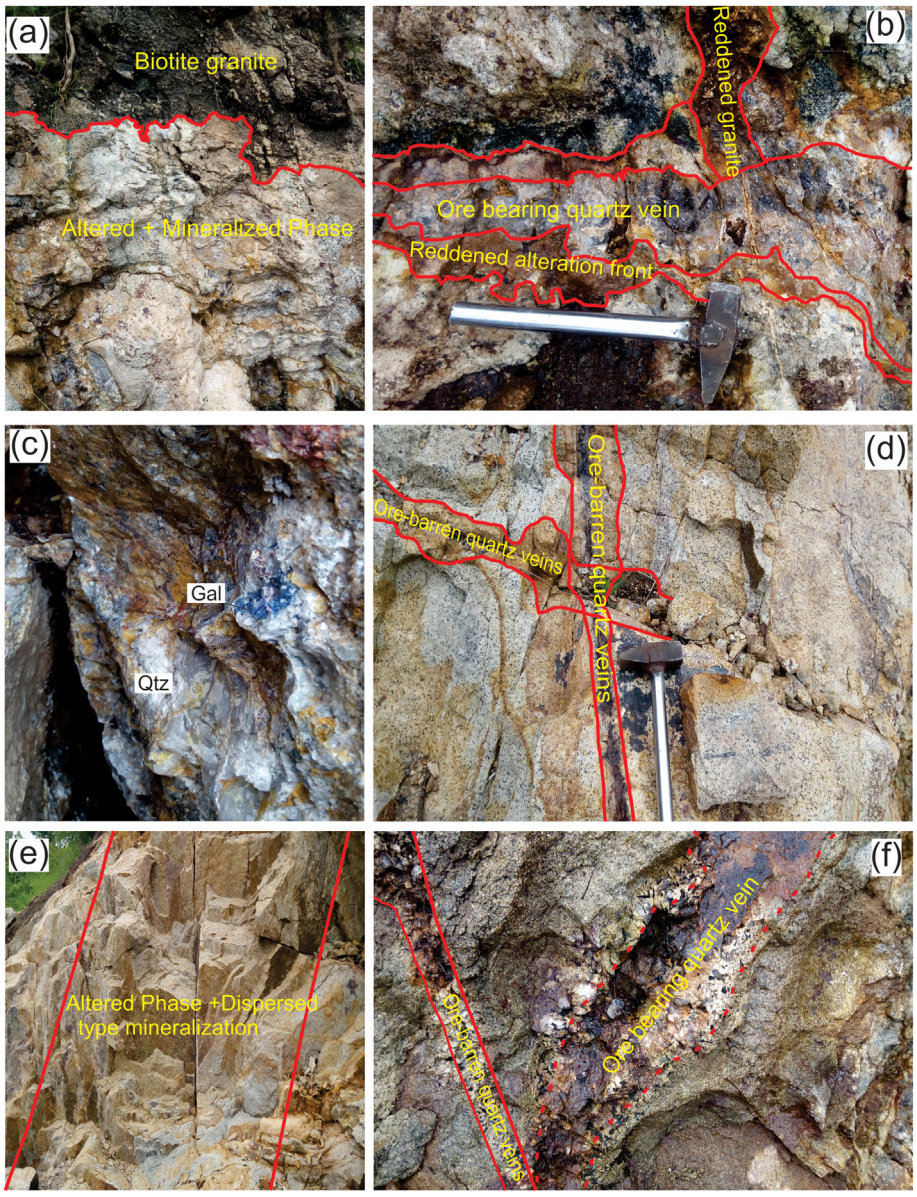

Fig. 3. Field occurrences of wall rocks, ore bearing quartz and alteration zones at the Jigawa Pb—Zn mineralization. (a) Field relationship between unmineralized and mineralized granites in the Jigawa Pb—Zn ore field; (b) structural relationship between ore bearing quartz veins and k-altered fronts; (c) galena bearing quartz vein from an ore bearing lode; (d) field relationship between ore bearing and ore barren quartz veins; (e) altered granitic phase associated with dispersed-type mineralization; (f) field relationship between ore bearing and ore barren quartz veins. Qz: quartz; Py: pyrite; Gal: galena; Chl: chlorite.

galena occur as replacement type ore bodies (Fig. 4i-j). Sample JK2A and 6A were taken from wall rock sections at the eastern end of the No. 1 ore vein. The galena occurs as overgrowths on quartz (Fig. 4k). Under an ore microscope, the samples are quartz-sulfide ore containing euhedral-subhedral galena and sphalerite (Fig. 4i-o) with accessory copper minerals (malachite). Zircon for U/Pb dating and Hf/Lu isotope analysis were extracted from six samples (CHR1, KLK1A, AT1A, AT1B, JK1A and JK6A). In addition, representative samples from ore bearing quartz veins, unmineralized and mineralized granites were selected for thin section preparation. Samples for zircon U/Pb dating were crushed to <250 μm using a vibrating agate mill. Zircon grains were extracted from the crushed samples using conventional density and magnetic separation techniques. The zircons were handpicked under a binocular microscope, mounted in epoxy resin and polished to expose the centre of each grain. Cathodoluminescence (CL) images of the zircon were captured using a scanning electron microscope (SEM) fitted with an energy-dispersive system (EDS) at the State Key Laboratory of Geological Processes and Mineral Resources (GPMR), China University of Geosciences (Wuhan). Using He gas, U/Pb zircon spot dating was carried out on an Analytik Jena PQMS Elite ICP-MS coupled with an ESI NWR 193-nm laser ablation system at SampleSolution Analytical Technology Co., Ltd. (Wuhan). NIST SRM610 and Zircon 91,500 were used as external standards (Supplementary Table 1). The trace element values of the standard samples have good correlation with reference values (Supplementary Fig. 1). Laser ablation spots were carefully selected to avoid fluid and mineral inclusions in the zircon grains. Laser frequency was 8 Hz with an ablation spot size of 32 μm and depth of 20–40 μm. Analytical conditions and procedure are based on those described by Yuan et al. (2008). ICP-MS-Data Cal software of Liu et al. (2008) was used for data calibration and corrections. Mean weighted average (MSWD) ages and Concordia diagrams were calculated and plotted using Isoplot software (Ludwig, 2003).

In-situ Lu/Hf isotope analysis was performed using a Neptune plus MC-ICP-MS coupled with a Geolas 2005 Excimer ArF laser ablation

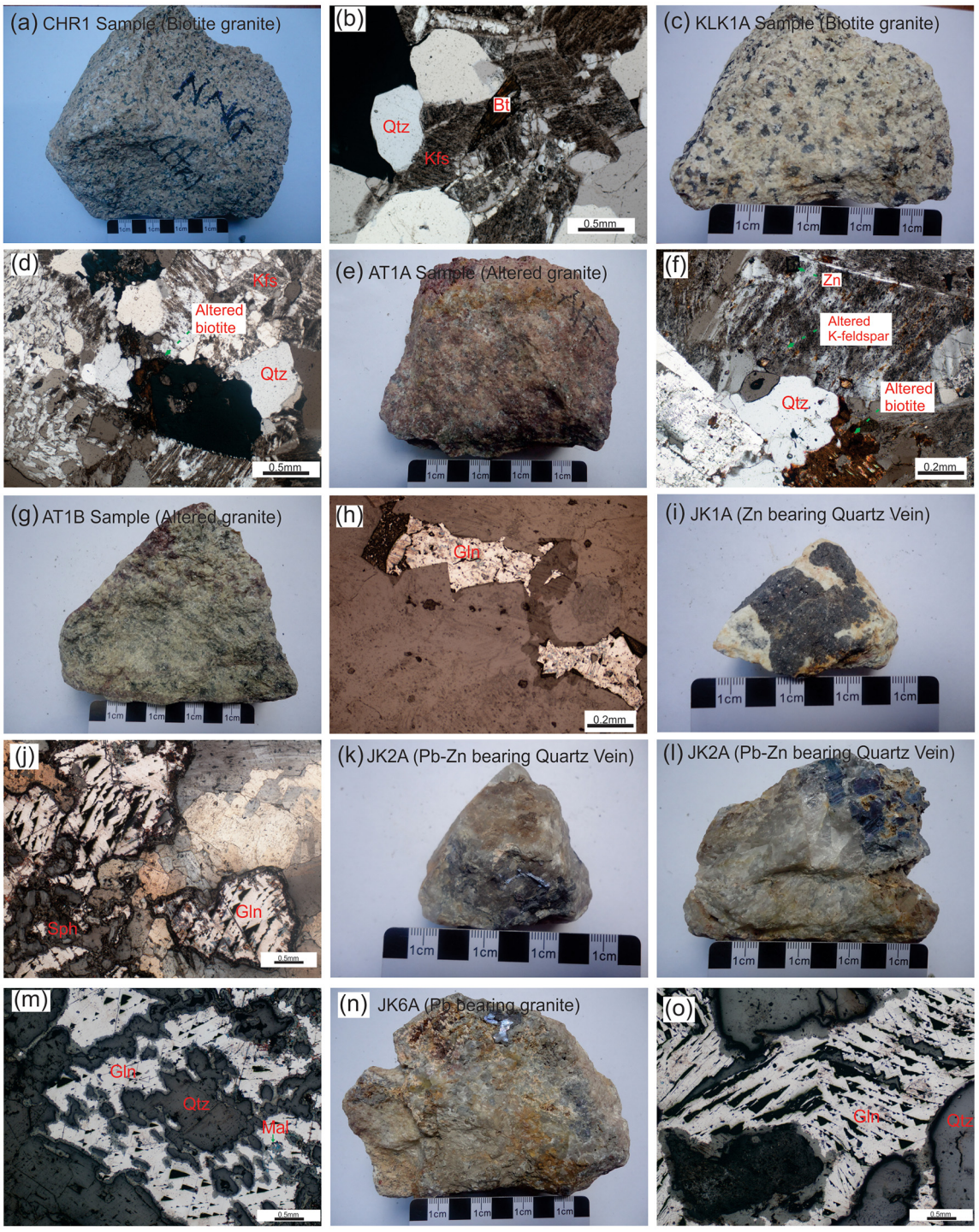

Fig. 4. Hand specimen images and photomicrographs of unmineralized and mineralized rock samples from the Jigawa Pb–Zn ore field. (a), (b): sample CHR1; (c), (d): sample KLK1A; (e), (f): sample AT1A; (g), (h): sample AT1B; (i), (j): sample JK1A; (k), (l), (m): sample JK2A; (n), (o): sample JK6A. Qtz: quartz; Bt: biotite; Kfs: K-feldspar; Sph: sphalerite; Gln: galena.

system at GPMR. Data acquisition was carried out for approximately 60s on laser spot situated adjacent to those for U/Pb dating. Two zircon standards (91500 and GJ-1) were analyzed to correct the Hf isotopic values, among which 91,500 was analyzed twice for every eight unknown samples and GJ-1 was measured twice every 20 unknowns. The total analysis yielded the mean $^{176}Hf/^{177}Hf$ values = 0.282308 ± 0.000021 for 91,500 (95% conf., $n = 24$) and =0.282000 ± 0.000027 ($n = 12$), respectively. These values are within uncertainty of already established values determined by GPMA of 0.282307 for 91,500 (Woodhead et al., 2004) and 0.282013 for GJ-1 (Hu et al., 2012). Based on values recommended by Machado and Simonetti (2001), Standard ratios of $^{176}Hf/^{175}Lu$ (0.0265) and $^{176}Yb/^{172}Yb$ (0.5886) were used to correct for isobaric interferences of ^{175}Lu on ^{176}Hf and ^{176}Yb on ^{176}Hf respectively. Present-day chondritic values of $^{176}Hf/^{177}Hf$ (0.2827) and $^{176}Lu/^{177}Hf$ (0.0332) proposed by Belousova et al. (2006) was used for epsilon Hf (εHf(t)) calculations. Single-stage Hf model ages (T_{MD1}) were calculated using the present-day depleted mantle ratios of $^{176}Hf/^{177}Hf$ (0.2832) and $^{176}Lu/^{177}Hf$ (0.0384) of Griffin et al. (2002).

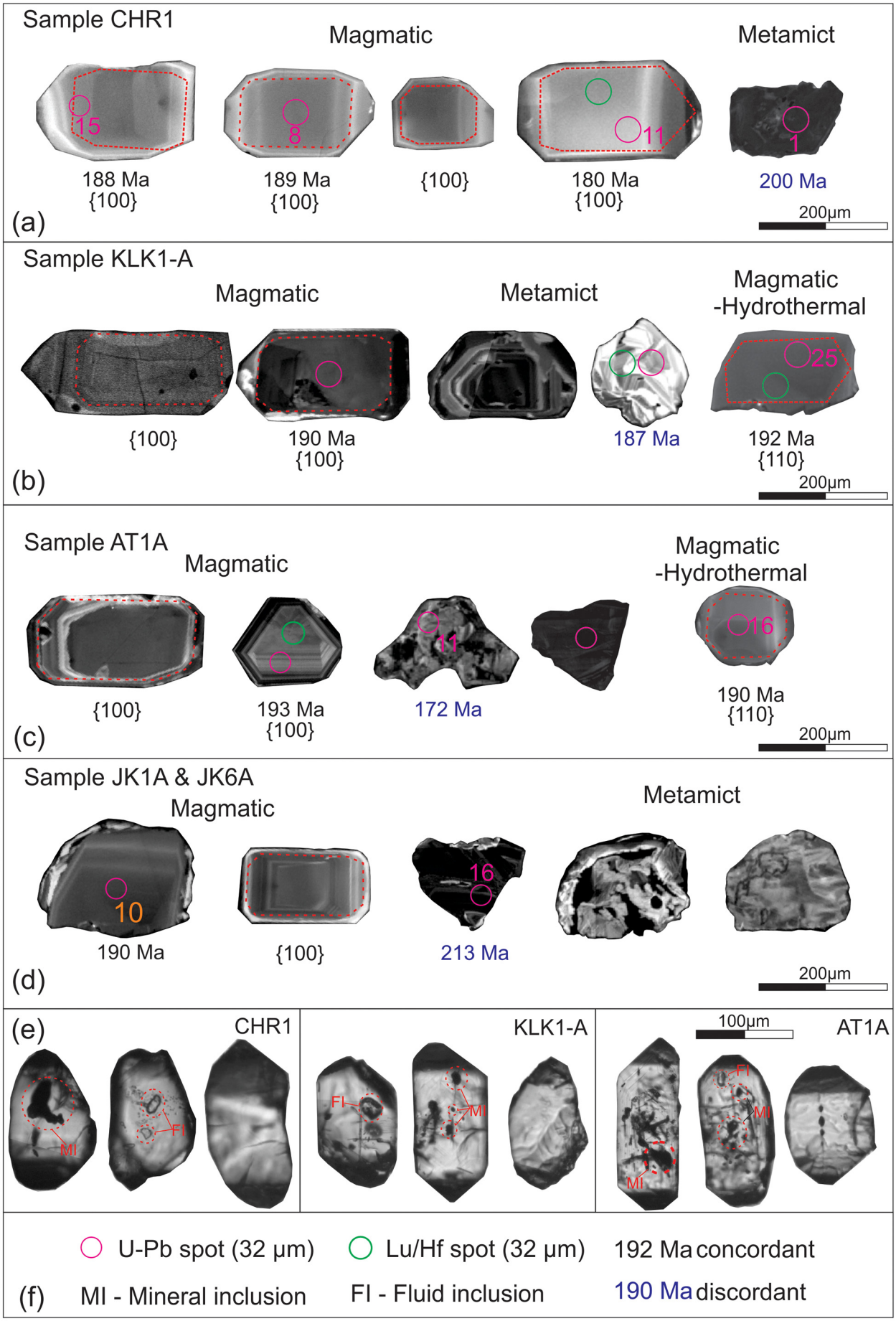
Sample CHR1
Magmatic
Metamict
15
8
11
1
188 Ma
{100}
189 Ma
{100}
{100}
180 Ma
{100}
200 Ma
200μm
(a)
Sample KLK1-A
Magmatic
Metamict
Magmatic
-Hydrothermal
25
{100}
190 Ma
{100}
187 Ma
192 Ma
{110}
200μm
(b)
Sample AT1A
Magmatic
Magmatic
-Hydrothermal
11
16
{100}
193 Ma
{100}
172 Ma
190 Ma
{110}
200μm
(c)
Sample JK1A & JK6A
Magmatic
Metamict
10
16
190 Ma
{100}
213 Ma
200μm
(d)
(e)
CHR1
KLK1-A
100μm
AT1A
MI
FI
MI
FI
FI
MI
MI
FI
MI
○ U-Pb spot (32 μm)
○ Lu/Hf spot (32 μm)
192 Ma concordant
(f)
MI - Mineral inclusion
FI - Fluid inclusion
190 Ma discordant

Crustal Hf model ages (T_{DMC}) were computed using the mean continental crust $^{176}Lu/^{177}Hf$ ratio (0.015) of Belousova et al. (2006).

4. Results

4.1. Zircon internal textures and morphology

Zircon from the unmineralized and mineralized suites in the Koluki-Burra orefield show variable morphologies and internal textures as observed in cathodoluminescence (CL), reflected and transmitted images (Fig. 5). Most of the zircon grains are 50–300 μm in diameter with length/width ratios of 1:1 to 3:1 (Fig. 5; also see Supplementary Fig. 2). For the unmineralized granites, zircon from Sample CHR1 are euhedral to anhedral in shape and show apparent oscillatory zoning; whereas those from sample KLK1A are bright to dark in color with weak oscillatory zoning. In the mineralized granites, zircon grains display a combination of bright crystals with clear zoning and metamict bright-dark grains with spongy textures. The zircon population in Sample AT1A, AT1B, JK1A and JK6A can be divided into three groups (magmatic, hydrothermally-altered and inherited zircon grains): 1) the first group are magmatic zircon grains which are euhedral to anhedral in shape and show apparent oscillatory zoning. However, some grains are composed of oscillatory zones flanked by un-zoned areas or other oscillatory zones with different CL brightness. 2): the second group of zircon grains are hydrothermally-altered zircon grains which are euhedral to subhedral in shape with dark CL luminescence. Under reflected and transmitted light images (Fig. 5d), the highly metamict zircon contain abundant inclusion indicative of significant hydrothermal re-working. 3): the third group of zircon grains (inherited zircons) are subhedral to anhedral grains (n = 2) with bright CL luminescence and show variable zonation structures. Detailed characteristics of each zircon population is given in Table 1.

4.2. Zircon U—Pb geochronology

Results of LA-ICP-MS U—Pb dating of zircon grains are listed in Supplementary Table 2. Zircon grains with low concordance (< 90%) were excluded from the following discussion and concordia plots. Concordant zircon grains ages greater than 220 Ma are interpreted to represent inherited zircon ages and, hence, were excluded from Concordia age calculations. Furthermore, magmatic zircon grains which have undergone slight Pb-loss were differentiated (Fig. 7a) and also excluded from Concordia age calculations. Two distinct groups of zircons (magmatic and hydrothermally altered zircon) have been identified in sample KLK1A. Magmatic zircon from KLK1A sample yield concordant ages of 192.1 ± 4.7 Ma (MSWD = 4.9, n = 5) (Fig. 6b). Group 2 zircon which shows signatures synonymous with hydrothermal zircon yield concordant ages of 192.4 ± 1.1 Ma (MSWD = 0.21, n = 4) (Fig. 6c). On the other hand, zircon grains from Sample CHR1 are principally magmatic zircon (Th/U = 0.42–0.80) and they yield a mean weight age of 186.2 ± 2.3 Ma (MSWD = 1.3, n = 7; Fig. 6a). Zircon from mineralized granites yield three distinct $^{206}Pb/^{238}U$ ages clusters (191–188 Ma, 181–178 Ma and 172–170 Ma). Sample ALT1A also contain two distinct zircon groups. Seven magmatic zircon grains constitute the first group which yield $^{206}Pb/^{238}U$ ages of 190.3 ± 1.7 (MSWD = 0.54, n = 7; Fig. 6d) and three hydrothermally altered zircon grains constitute the second group which yield $^{206}Pb/^{238}U$ concordant ages of 189.0 ± 1.3 Ma (MSWD = 3.1, n = 3; Fig. 6e). A single hydrothermal grain gave $^{206}Pb/^{238}U$ concordant age of 172.2 ± 2.8 Ma. Four magmatic zircon grains (Fig. 6f) from Sample AT1B yield a concordant age of 188.6 ± 1.2 Ma (MSWD = 0.15, n = 4). However, a single magmatic grain yields concordant age of 175.8 ± 2.1 Ma. Zircon grains from Sample JK1A and 6A are predominantly magmatic (Th/U = 0.35–0.84) and yield a concordant age of 191.7 ± 0.7 Ma (MSWD = 3.6, n = 10; Fig. 6g); whereas those from Sample JK6A yield a weighted mean age of 191.3 ± 2.5 Ma (MSWD = 1.9, n = 9; Fig. 6h).

4.3. Zircon trace element compositions

Trace element compositions of zircon from the studied granites are given in Supplementary Table 3. Trace element content varies significantly between the unmineralized and mineralized granites. In the unmineralized samples (KLK1A & CHR1), Group 1 zircons are characterized by low ΣREE (< 3000 ppm), Ti (< 5 ppm), Y (< 2000 ppm), Hf (< 20,000 ppm), Th (< 2500 ppm) and U (< 1000 ppm). On chrondite-normalized REE diagrams, most zircons show positive Ce anomalies and negative Eu anomalies (Fig. 8a-d). However, three zircon grains from Sample KLK1A show no distinct Ce but large negative Eu anomaly suggestive of plagioclase fractionation prior to zircon growth (Fig. 8b). Compared to magmatic zircon, hydrothermal zircon from Sample KLK1A show flat HREE with relatively weak negative Eu anomaly (Eu/Eu* = 0.06–0.18) and positive Ce anomaly (Ce/Ce* = 2.18–23.9; Fig. 8b). Trace element and REE distribution for both zircon groups in the mineralized rocks also varies widely, with Y values of 226–5379 ppm, Hf contents of 7600–23,300 ppm, Th contents of 65–1012 ppm, U contents of 130–1274 ppm, and total REE from 556.7–3726 ppm. However, they exhibit negative Eu anomaly (Eu/Eu* = 0.02–0.13) with positive yet variable Ce anomaly (Ce/Ce* = 1.8–1752).

4.4. Zircon Hf isotopes

Thirty-five representative zircon spots were selected for Hf isotopic analysis (Supplementary Table 4). Zircon from the unmineralized granites (sample CHR1 & KLK1A) show a narrow range of εHf(t) (−10.3 to −5.1), $^{176}Lu/^{177}Hf$ (0.00005–0.002589), $^{176}Yb/^{177}Hf$ (0.011314–0.090049) and variable $^{176}Hf/^{177}Hf$ (0.282450–0.282516) values. Calculated two-stage Hf model ages for the granites range from 1064 to 1258 Ma and from 1558 Ma to 1887 Ma for T_{DM1} and T^{C}_{DM}, respectively. Zircon hosted in the mineralized suites also show variable Lu/Hf isotopic ratios. Values range from $^{176}Hf/^{177}Hf$ (0.282461–0.282538), $^{176}Lu/^{177}Hf$ (0.000476–0.003016), $^{176}Yb/^{177}Hf$ (0.016712–0.107433) and εHf (t) (−6.9 to −4.4). Calculated two-stage Hf model ages for the granites range from 1059 to 1209 Ma and from 1517 Ma to 1769 Ma for T_{DM1} and T^{C}_{DM}, respectively. Due to standard fLu/Hf values (< −0.9), calculated Hf T^{C}_{DM} modal ages are considered reliable estimates of crustal residence times.

5. Discussion

5.1. Timing of magmatic-hydrothermal activities in the Ningi-Burra complex

New zircon data presented in this study allows for precise timing of magmatic activities in the Ningi-Burra suites and its implication for the evolution of the ring complex. Compared to Rb/Sr ages (183 ± 7.0 Ma) from the eastern part of the Ningi-Burra complex (Rahaman et al., 1984), Zircon U/Pb ages for the western massifs cluster around 194–191 & 188–186 Ma (Supplementary Table 2). The 188–186 Ma ages suggests a later magmatic event in the Koluki-Burra centre. However, our discussion of the wide ranges of ages obtained in this study bear on the precision of LA-ICP-MS techniques, which range from 2 to

Fig. 5. Selected CL-images of analyzed zircon grains from samples (a) KLK1A, (b) CHR1, (c) AT1A, JK1A & JK6A and (e) Representative transmitted and reflected light images of zircons, showing the distribution of fluid/mineral inclusions.

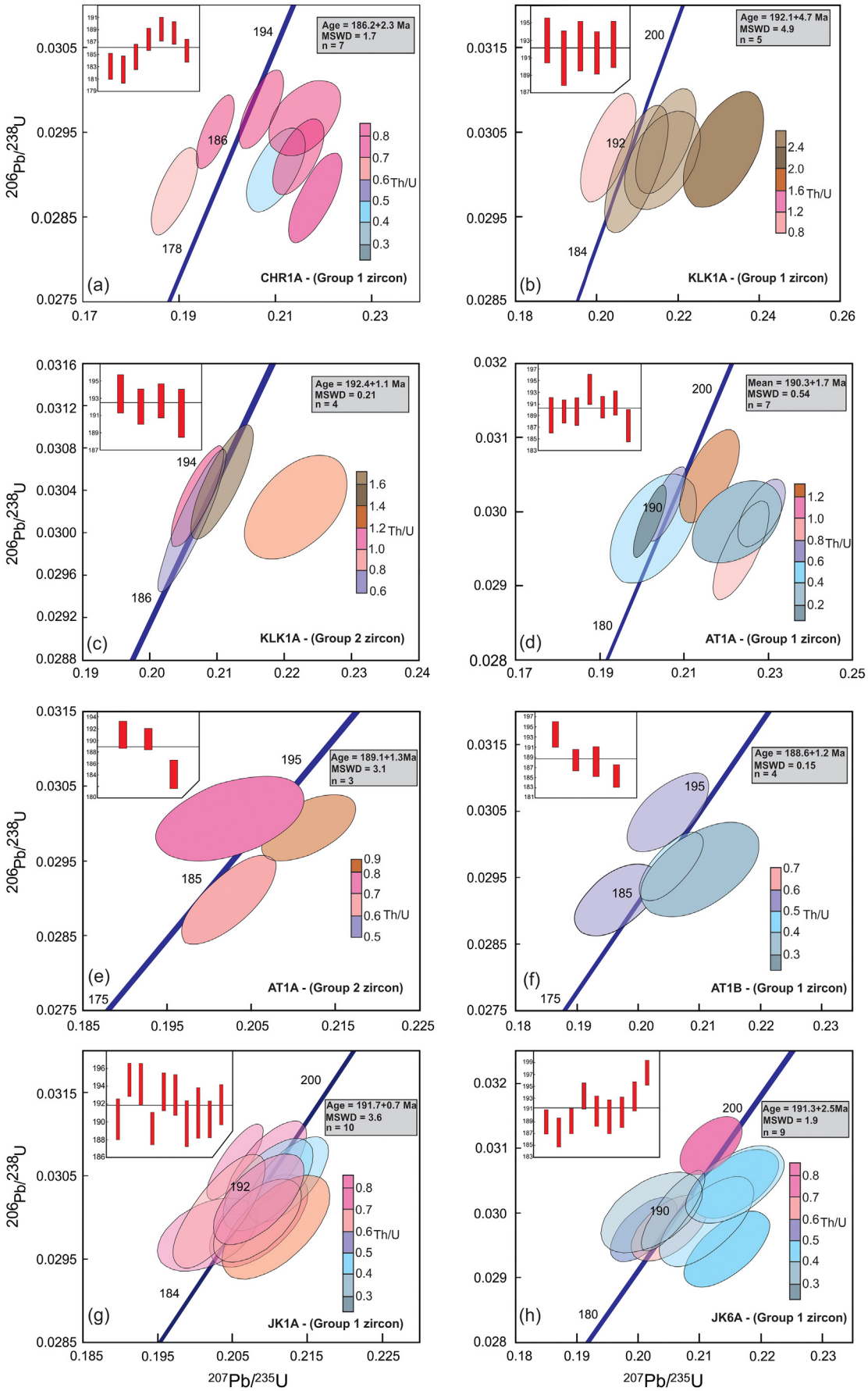

Fig. 6. U—Pb concordant ages of different zircon groups in samples (a) CHR1, (b-c) KLK1A, (d-e) AT1A, (f) AT1B, (g) JK1A and (h) JK6A from the Jigawa Pb—Zn mineralization. Group 1 zircons = magmatic zircons and Group 2 zircons = hydrothermally altered zircons.

Table 1
Major distinct characteristics of zircon types from the Jigawa Pb—Zn deposit.

Character/type	Magmatic	Hydrothermally-altered	Inherited
Size	50–300 μm	50–200 μm	100–150 μm
Morphology	Euhedral & anhedral Prisms {100} & {110}	Euhedral & subeuhedral Prisms {110}	Subhedral & anhedral Prisms {100}
Optical appearance	Transparent and colorless	Murky-brown opaque	Transparent and colorless
CL appearance	High intensity Clear zoned texture	Low intensity No zoned texture	High intensity Variable zoned textures
Formation mechanism	Early and late-stage magmatic melt	Early magmatic melt and altered by hydrothermal fluid	Mostly ancient magmatic melt (distinct zircon ages)
Internal structure	Inclusion-poor Fracture-poor	Inclusion-rich Fracture-rich Spongy texture	Inclusion-poor Fracture-poor
Geochemical feature	Moderate Eu anomaly Strong Ce anomaly Depleted in LREE Low common Pb content	Strong Eu anomaly Weak Ce anomaly Strongly enriched in U, Th, Y, REE, Nb Moderately enriched in Ti, Pb, Hf, Ta High common Pb content & varying degree of radiogenic Pb loss	Moderate Eu anomaly Strong Ce anomaly Depleted in LREE Low common Pb content
Zircon grain U/Pb ages	192–185 Ma	191–172 Ma	517–604 Ma
Lu/Hf isotope signature	−5.1 to −6.8	−5.7 to −10.3	–

4% (Klötzli et al., 2009). Nevertheless, we limit our characterization of the magmatic-hydrothermal episodes in the Jigawa Pb—Zn deposit to the main 192–190 Ma event for the Koluki-Burra biotite granites. Timing hydrothermal events using U/Pb dating of hydrothermal zircon have been widely applied to Au (Claoué et al., 1990), Sn—W (Jiang et al., 2019a; Jiang et al., 2019b; Li et al., 2014; Li et al., 2018) and Cu—Zn (Zhu et al., 2016) mineralizations. Complex multi-stage processes have been recognized elsewhere as crucial to the formation of

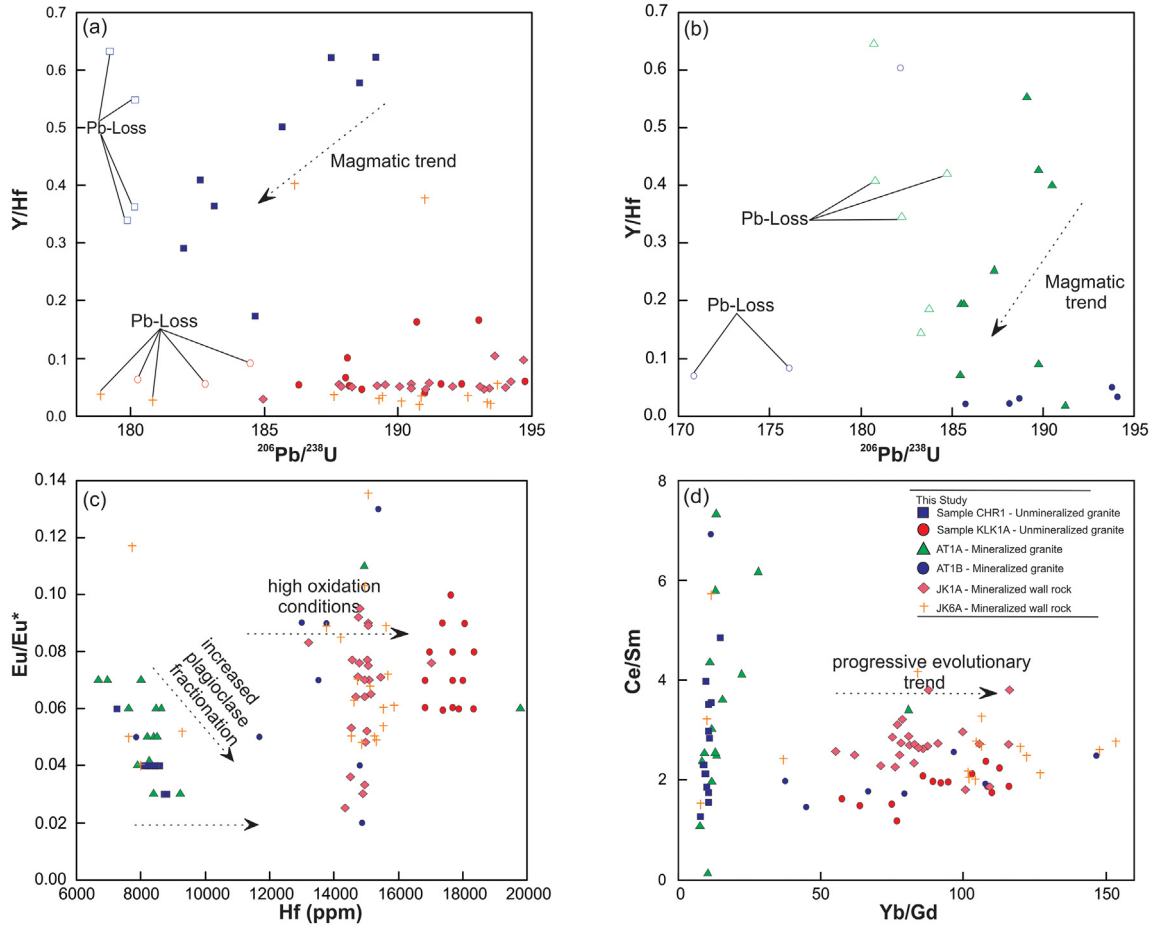

Fig. 7. Zircon trace element assay of plutonic zircon vs altered zircon which have suffered slight Pb-loss. (a-b) $^{206}Pb/^{238}U$ vs. Y/Hf for CHR1 & KLK1A; (b) $^{206}Pb/^{238}U$ vs. Y/Hf for AT1A & AT1B. Plots of (c) Eu/Eu* vs Hf (d) Ce/Sm vs Yb/Gd for zircon grains from the Jigawa Pb—Zn mineralization. Open circles represent grains with slight Pb loss.

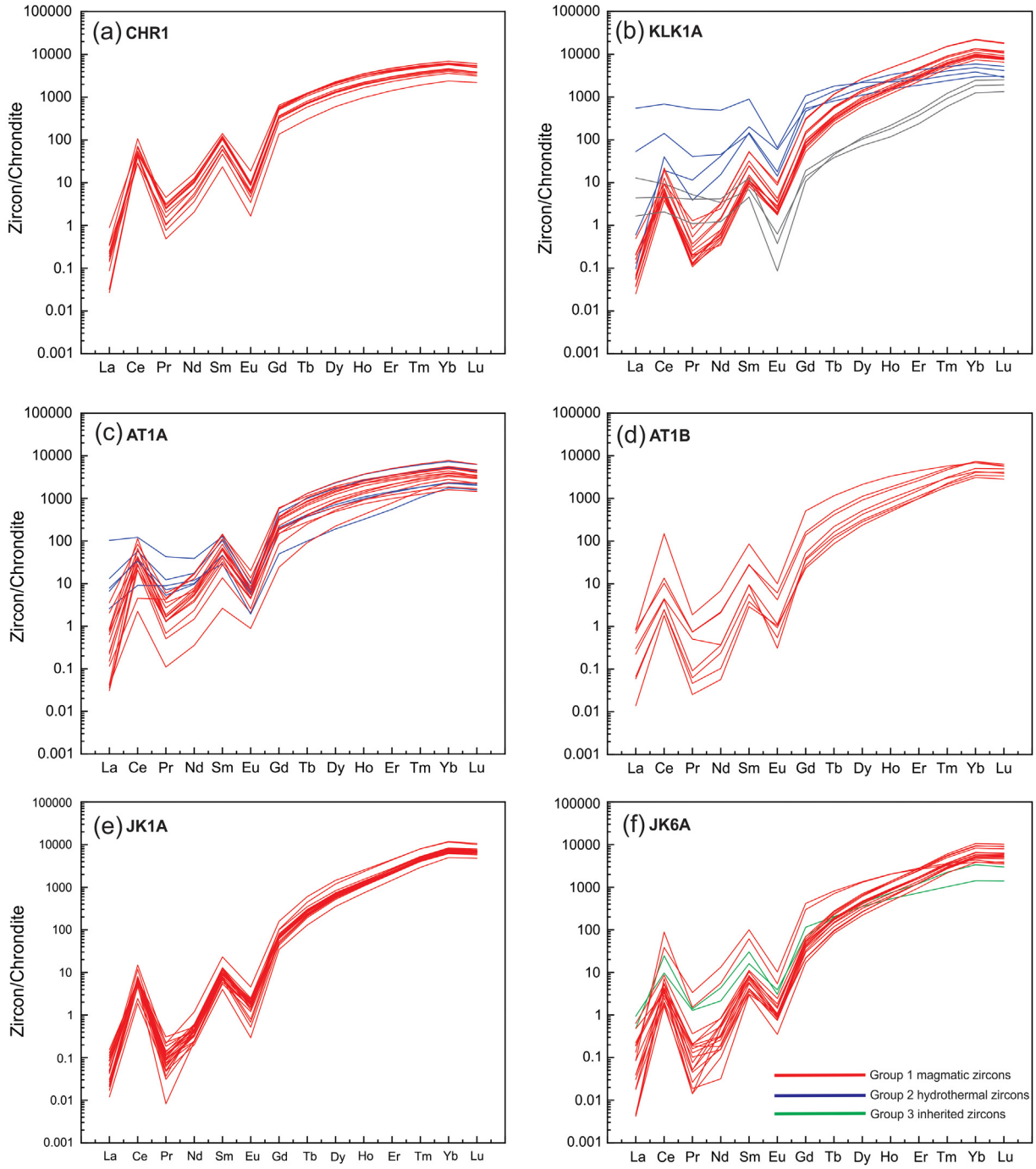

Fig. 8. Chondrite-normalized REE patterns for samples (a) CHR1, (b) KLK1A, (c) AT1A, (d) AT1B, (e) JK1A and (d) JK6A from the Jigawa Pb–Zn mineralization. Normalized values for chondrite are from Taylor and McLennan (1985).

large ore mineralization systems (Jiang et al., 2019b; Li et al., 2018). Magmatic and hydrothermally altered zircon in sample KLKIA and Sample ATIA yield coeval ages 192 to 190 and 192 to 189, respectively. This suggest that the mineralization event in the Jigawa suites took place shortly after the emplacement of the granites. As mentioned earlier, a few zircon grains (including both magmatic and hydrothermal) yielded younger $^{206}Pb/^{238}U$ ages ranging from 185 to 172 Ma (concordance > 90%). Correlation of trace elements variation (Y/Hf) as a function of time is useful in constraining the evolution of coeval zircons in a closed magmatic system (Schoene et al., 2010). Perturbed magmatic zircon population do not show compatible evolutionary trends with coeval magmatic grains in all samples (Fig. 7a-b). This suggests that the perturbed grains are magmatic zircon that have undergone some degree of Pb-loss, and hence, their ages cannot be interpreted to represent granite crystallization age. Concordant hydrothermal grains (184–170 Ma) may be related to hydrothermal resetting and slight radiogenic Pb-loss due to the low degree of hydrothermal alteration in the Koluki-Burra centre.

5.2. Source of magma and Pb—Zn mineralization in the Ningi-Burra complex

Magma source of granites can be constrained using distinct zircon trace elements and Hf isotope signatures which are indicative of different

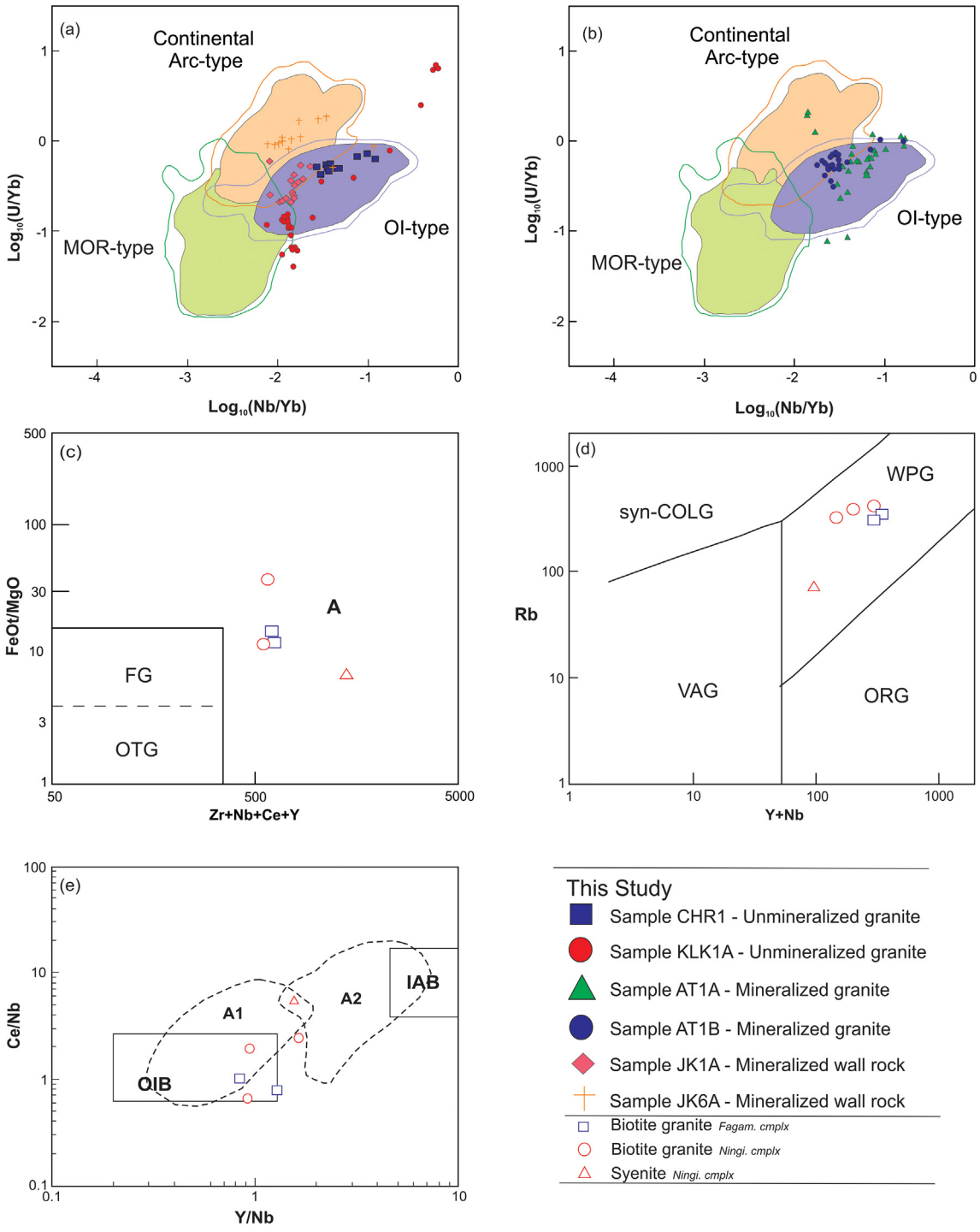

Fig. 9. (a-b) Granite discrimination plots based on zircon trace element; (c-e) comparative data based on trace element distribution from whole rock analysis. Data from Batchelor and Bowden (1986).

magma sources and evolutionary history. In particular, trace element data have proved to be a suitable tool for distinguishing distinct granitic rock suites (Pearce et al., 1984). Discrimination plots proposed by Grimes et al. (2015) for differentiating granite provenance based on zircon trace element chemistry was applied for the Jigawa zircon. The zircon from the unmineralized and mineralized granites plot within the field of Ocean Island (OI) type A-type granites (Fig. 9a-b), which is in agreement with whole-rock tectonic plots (Fig. 9c-e) from this complex and adjacent A-type complexes (Girei et al., 2019; Kamaunji et al., 2020; Kinnaird, 1985).

Lu—Hf isotope systems in zircon is considered to be a reliable tool in delineating magma and fluid sources in magmatic rocks (Kemp et al., 2006). Further constraints on magma source and distinct magmatic and hydrothermal processes during the evolution of granites can be drawn from isotopic signatures. Due to elevated concentrations of Hf in zircon and its fractionation relative to Lu, zircon Lu/Hf isotopic ratios are considered reflective of mantle-crust differentiation processes (Kemp et al., 2007). For granites from the Jigawa Pb—Zn ore field, unmineralized suites from the Koluki-Burra centre display a wide range of zircon εHf(t) values ranging from −4.9 to −10.3

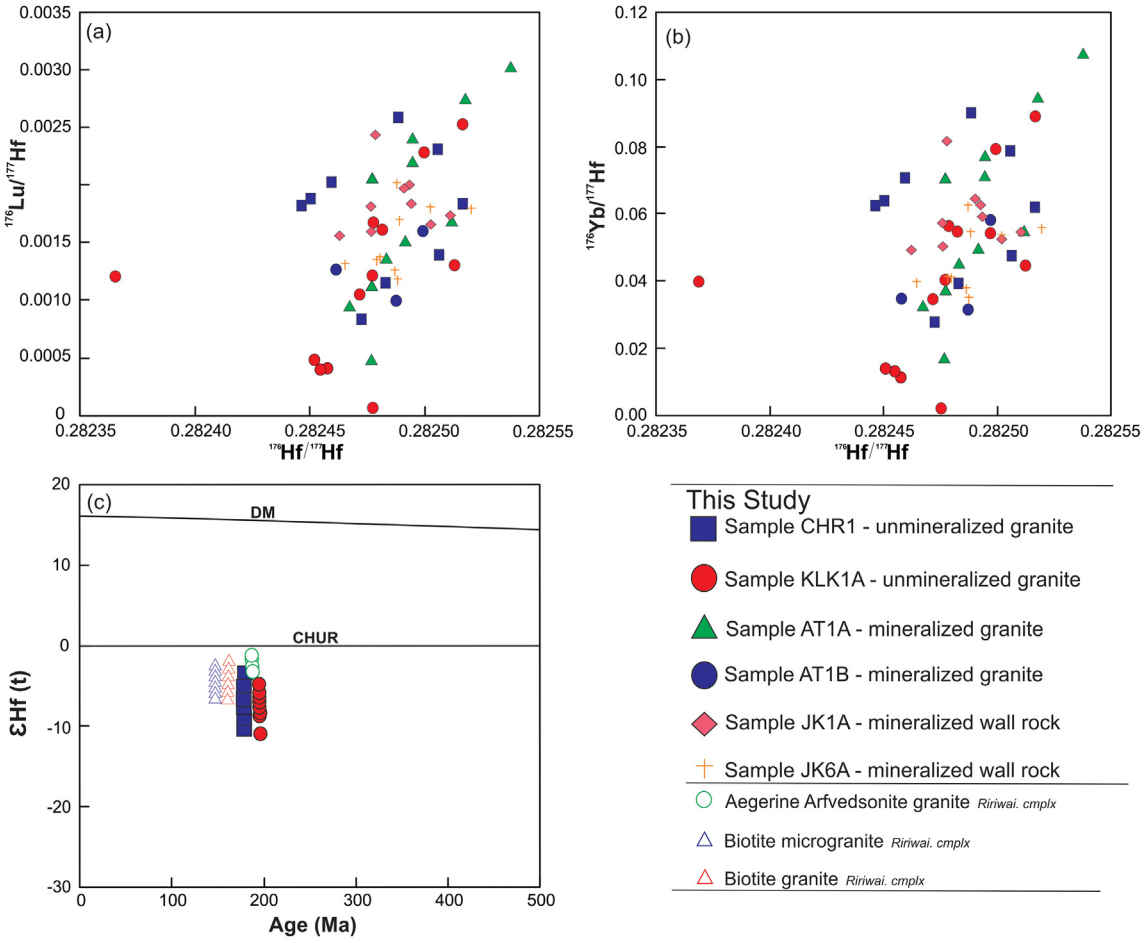

Fig. 10. Plots of (a) $^{176}Lu/^{177}Hf$ vs. $^{176}Hf/^{177}Hf$, (b) $^{176}Yb/^{177}Hf$ vs. $^{176}Hf/^{177}Hf$ and (c) εHf(t) vs age for the zircon grains from the Jigawa Pb—Zn mineralization.

(Supplementary Table 4). Calculated Hf model ages for the Ningi-Burra granite suggest magma interaction with crustal material of Paleoproterozoic to Mesoproterozoic ages (1.2–1.7 Ga). These crustal materials are most likely the basement complex rocks in the region. Moreover, the crustal model age is also in agreement with Pb/Pb slope array ages (1.8 Ga) for other Nigerian Younger granite complexes (Dickin et al., 1991). Furthermore, εHf(t) values for the granites plot below CHUR, this signature likely reflects parental melts largely derived from lower crustal sources with some contribution from the upper mantle (Fig. 10c) for the Ningi-Burra biotite granites. Previously reported whole-rock Sm—Nd, Rb—Sr and zircon Lu—Hf isotopic data for some anorogenic complexes also suggests, for the biotite granites in the Nigerian Younger Granite province, an enriched mantle-derived parental melt that has undergone significant crustal contamination (Dickin et al., 1991; Girei et al., 2019) or partial melting of crustal sources with contributions from the mantle (Girei et al., 2020). However, the Lu—Hf isotope data of the granites (this study) is more consistent with magma derivation from largely crustal source(s). Nonetheless, the presence of mafic rocks in the Ningi-Burra complex (Fig. 2a-b) suggests heat and material contribution from the mantle (Turner and Bowden, 1979). It can be inferred therefore that the rock associations in Centres 1 and 2 and those of Centre 6 may have been derived from partial melting of crustal sources with contributions from the mantle (Turner and Bowden, 1979).

Lu—Hf systems in zircon are fairly resistant to hydrothermal alteration episodes (Thompson et al., 2008). Hf remains stable relative to Lu and Yb which become highly mobile during hydrothermal phases associated with zircon alteration (Thompson et al., 2008; Valley et al., 2010). The $^{176}Hf/^{177}Hf$ ratios is similar in the magmatic and hydrothermally altered zircons from the Jigawa biotite granites (Fig. 10a-b). However, $^{176}Lu/^{177}Hf$ (up to 0.003) and $^{176}Yb/^{177}Hf$ (up to 0.107) ratios are markedly higher in samples with hydrothermally altered zircons (KLK1A and AT1A) compared to samples (CHR1 and AT1B) primarily associated with magmatic zircons (Fig. 10a-b). The overlap in εHf (t) values in the magmatic and hydrothermally altered zircon grains from the Jigawa Pb—Zn orefield (Table 1; Supplementary Table 4) suggest that the mineralizing fluids were sourced from the granites. This is in agreement with finding from previous studies based on whole-rock Sr—Nd and oxygen isotopes (Kinnaird, 1985; Kinnaird et al., 1985).

5.3. Petrochemical characteristics of zircon from the Ningi-Burra Complex

Based on morphological features, magmatic zircon are characterized by clear oscillatory zoning when compared with hydrothermal zircon which display weak or no oscillatory zoning. Moreover, hydrothermal zircon typically possess spongy and ragged textures and have numerous mineral inclusions (Hoskin, 2005; Jiang et al., 2019b; Li et al., 2014; Pelleter et al., 2007). Compared to magmatic zircon, hydrothermal zircon are relatively enriched in non-formula elements (Hf, U, Y Th, LREE, etc.) and show weak Eu and Ce anomalies (Hoskin, 2005; Li et al., 2018). Moreover, trace element distribution is significantly higher in hydrothermal zircon when compared to magmatic zircon (Hoskin, 2005; Kebede et al., 2007). Compared to HREE, LREE's are highly mobile in hydrothermal phases (Sheard et al., 2012) and are then concentrated in metamict and hydrothermal zircon grains (Hoskin, 2005). In the Jigawa Pb—Zn field, hydrothermally altered zircon are typically

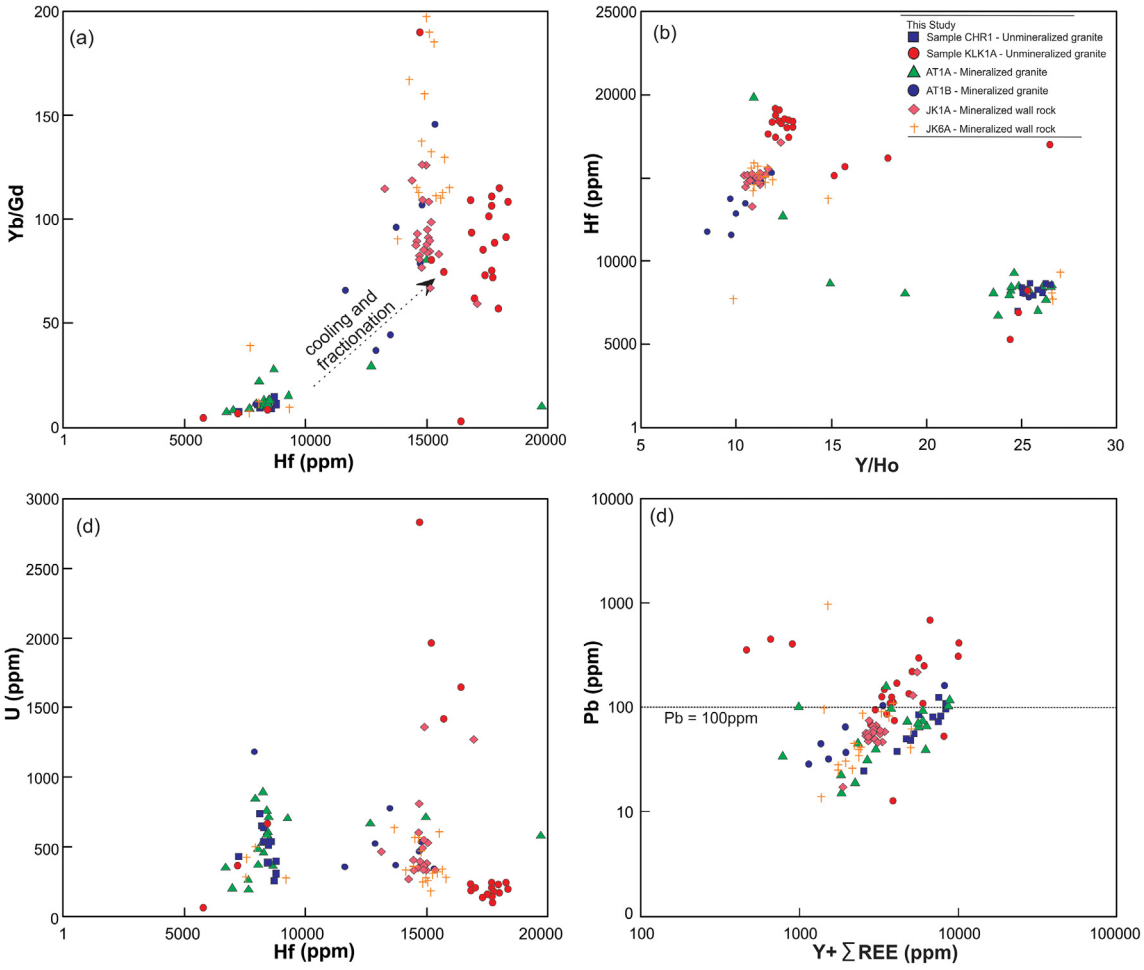

Fig. 11. Plots of (a) Yb/Gd vs. Hf, (b) Hf vs. Y/Ho, (c) Hf vs. U, and (d) Pb vs. Y + ΣREE for zircon grains from the Jigawa Pb–Zn mineralization.

enriched in LREE when compared to magmatic zircon (Fig. 8b-c; Fig. 12c-d). Trace element distribution (REE + Y) against total Pb provides further evidence for element incorporation into the zircon lattice (Fig. 11d). The positive trend noted for the Jigawa granites demarcates magmatic from hydrothermally altered zircons. The light rare element index (LREE-I = Dy/Nd + Dy/Sm) of Bell et al. (2019) is another viable tool for tracking alteration and contamination in magmatic zircon. Magmatic zircon from the unmineralized and mineralized granitic suites possess high LREE-I values indicative of limited aqueous alteration (Bell et al., 2019). LREE-I values (Supplementary Table 3) in group 1 zircon (magmatic) vary from 554 to 1123 in KLK1A, 95–200 in CHR1, 83–485 in AT1A, 209–2382 for AT1B, 435–1775 in JK1A, and 153–3872 in JK6A. On the other hand, group 2 zircon (magmatic-hydrothermal) contain low LREE-I values (KLK1A = 6–91 and AT1A = 19–81). Furthermore, discrimination plots proposed by Hoskin (2005) show the zircon from the Jigawa Pb—Zn field can be distinguished into Group 1 (magmatic) and Group 2 (hydrothermally altered) zircon (Fig. 12a-b). According to Anderson et al. (2008), trace element and REE redistribution during zircon metamictization are largely controlled by coupled dissolution and reprecipitation reactions along microfractures. In sample AT1A, sharp reaction fronts between the recrystallized and protolithic cores (Fig. 5a) provide evidence for dissolution–reprecipitation as a major alteration process in the Jigawa Pb—Zn deposit. Dissolution of the ΣREE-rich magmatic zircon is linked to coupled precipitation of ΣREE-poor hydrothermal zircon grains in an inward moving fluid (Soman et al., 2010). Zircon grains from Sample AT1B (see Electronic Supplementary Material Fig. 2) show deformation associated with weak fluid-fluid interaction. Therefore, alteration appears to be mild and have only deformed the lattice of the zircon resulting in Pb-loss. Based on available evidence, we preclude zircon precipitation from Zr- and Pb- rich fluids as a primary formation mechanism for hydrothermal zircon in the Jigawa Pb—Zn deposit. However, we propose magmatic zircon diffusion, zircon-fluid reaction, dissolution and reprecipitation as the driving mechanism for the formation of hydrothermally altered zircons in the Jigawa Pb—Zn deposit.

Ti-in-zircon thermometry, as proposed by Watson and Harrison (2005), has been identified as a reliable tool for constraining zircon crystallization and host magma temperature (Li et al., 2014). However, Ti concentration in zircon may be affected by lattice defect and dissolution-recrystallization process, giving rise to anomalously high Ti in zircon (Fu et al., 2008). High Ti may also concentrate in micro-inclusions in zircon and can be sampled by laser ablation (Harrison and Schmitt, 2007). Therefore, high contents of Ti (Supplementary Table 3) in metamict and fluid-altered (hydrothermal) zircon from the unmineralized sample KLK1A and mineralized rocks in the Jigawa Pb—Zn deposit (Samples AT1A and AT1B) are considered unrelated to initial Ti concentrations and the application of Ti-in-zircon thermometry is considered inappropriate. Ti-in-zircon values for magmatic zircons from the Jigawa Pb—Zn deposit yield average temperature of 605 °C for zircons from unmineralized granites, 645 °C for zircon from mineralized granite, and 600 °C for zircon from the wall rock. These values are significantly lower than the values computed using zircon saturation temperatures (Average temperature – 804 °C) from the whole-rock data reported by Batchelor and Bowden (1986). This variation is likely explained by variations in aTiO2 and aSiO2 conditions during crystallization of early and late zircons from the granitic melts. Moreover, according to Schiller and Finger

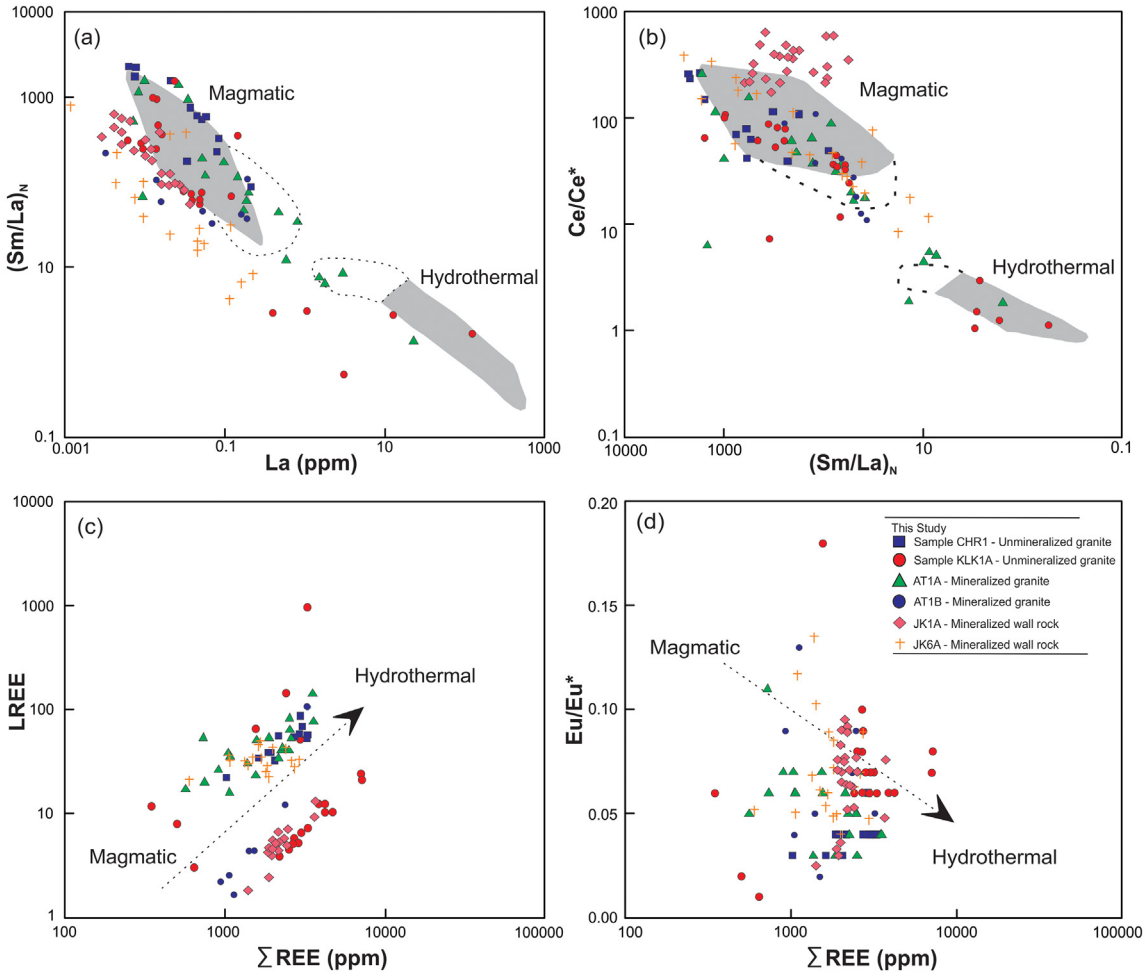

Fig. 12. Hydrothermal zircon discrimination plots of (a) SmN/LaN vs. Ce/Ce* diagram; (b) La vs. SmN/LaN diagram; (c) ΣREE vs. LREE and (d) ΣREE vs. Eu/Eu* values in zircon grains from the Jigawa Pb—Zn mineralization. (a)-(d) after Hoskin (2005),

(2019), calculated temperature using Ti-in-Zircon thermometry for A-type granites are usually 30-150 °C lower than their average crystallization temperatures. Importantly, Pupin (1980) has shown that zircon growth are highly dependent on temperature and pressure conditions of the melt. Therefore, crystal form/prism of zircon can be interpreted as reflective of magma temperatures (Belousova et al., 2002; Hoskin and Schaltegger, 2003). For the unmineralized KLK1A sample, the most developed crystal prisms in the magmatic zircon is the "100" prism which constrain the biotite granites as forming from high temperature (>700 °C) melts (Hayashi and Shinno, 1990). This view is supported by whole rock zircon saturation temperature measurements from other ring complexes in the Nigerian Younger Granite province (Bowden and Kinnaird, 1984; Kinnaird, 1985). Conversely, hydrothermal zircon from Sample KLK1A primarily exhibit "110" prism pointing to late-stage magmatic-hydrothermal origin. For the mineralized rocks, varying degree of metamictization has preserved both prism types (Fig. 5a). Most magmatic zircon still preserve well developed "100" prisms (Fig. 5a) indicating a higher temperature regime before fluid alteration responsible for rare metal enrichment in the granites.

5.4. Magmatic-hydrothermal evolution of the Jigawa Pb—Zn Ore field

Several ratios (e.g., Zr/Hf and Yb/Gd) in zircon are considered reflective of magmatic-hydrothermal processes have been used as robust tools for tracking the degree of evolution in granites (Breiter et al., 2014; Castiñeiras et al., 2011). Based on this, Zr/Hf values of >55 are considered typical of less fractionated granites that are devoid of mineralization, whereas Zr/Hf values of 25–55 are typical of moderately fractionated granites. In contrast, highly fractionated granite associated with mineralization display very low Zr/Hf values (Bau, 1996). The Zr/Hf values for the unmineralized sample CHR1 range from 70.8–84.0 while those from Sample KLK1A and mineralized samples (AT1A, AT1B, JK1A and JK6A) range from 34.12 to 111.82 and from 30.85 to 90.64, respectively. This indicates the increasing degree of fractionation from unmineralized granites to the mineralized granites in the Ningi-Burra complex. Because zircon are the primary reservoir for both Zr and Hf in granitic systems, crystallization of zircon controls Zr/Hf ratios and reflects degree of fractionation of the parental melt (Claiborne et al., 2006). Therefore, low Zr/Hf in zircon reflects crystallization from highly differentiated melts (Linnen and Keppler, 2002). The increased in the size of Eu anomaly with decreasing Hf content is interpreted to reflect feldspar fractionation during magma evolution (Castiñeiras et al., 2011; du Bray et al., 2011). Eu/Eu* vs Hf for the granites from the Jigawa Pb—Zn ore field show progressive plagioclase fractionation for the CHR1 and AT1A suites (Fig. 7c). A similar trend is notable for Hf values against Yb/Gd values (Fig. 11a), the positive correlation trend is considered indicative of progressive cooling and feldspar differentiation during magmatic evolution for the Jigawa granites (Barth and Wooden, 2010; Claiborne et al., 2010). Furthermore, increased differentiation in sample KLK1A based on Ce/Sm against Yb/Gd values suggest increased crustal contribution relative to Samples CHR1 and AT1A (Fig. 7d).

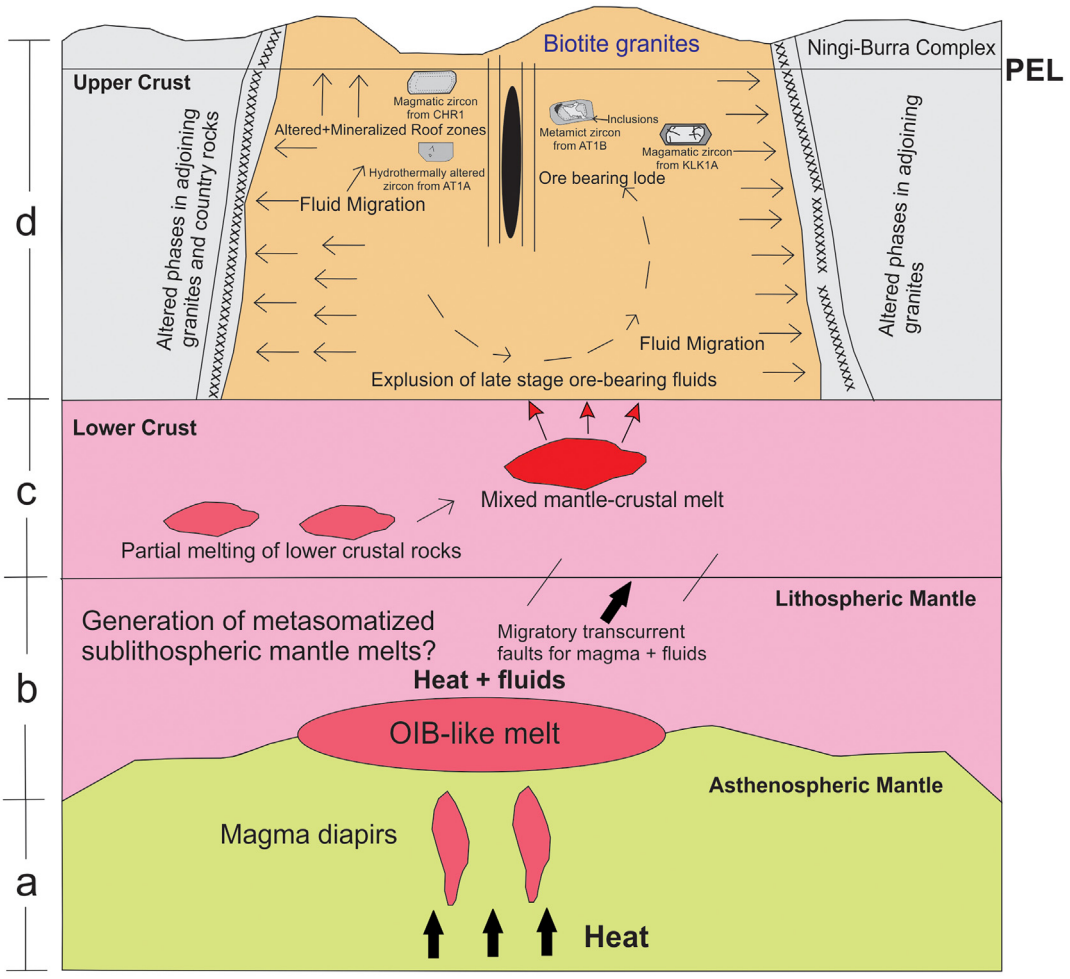

Fig. 13. A magmatic-hydrothermal model showing the genesis of the Jigawa Pb—Zn mineralization (a) mantle-derived magma undergoes crustal contamination; (b) Metasomatism of the melt precedes migration into the crust triggered by high temperature and pressure regimes during transcurrent fault movement of the plate; (c) fractional crystallization leads to generation of highly evolved granitic suites with hydrothermal phases generated during late-stages of magmatic emplacement drive ore-bearing and zircon altering fluids phases through the rock; (d) metals are deposited as disseminations and in ore bearing quartz veins. PEL = Present erosion level.

Several studies have demonstrated that the trace element concentrations in zircon are usually modified during fluid-rock interaction related to the formation of economically significant mineralization (Geisler et al., 2003a; Rubin et al., 1993). During hydrothermal alteration episodes, incorporation of Ca, Al, Fe, Mn, LREE and depletion of Zr, Si and radiogenic Pb is common for Th—U rich zones in zircon (Geisler et al., 2003b; Yang et al., 2014). None and/or limited incorporation of Pb in altered zircon has been demonstrated by several workers (Harlov et al., 2012; Lewerentz et al., 2019). This attests to the viability of dating altered and/or re-crystallized zircon to constrain the timing of metasomatism and/or mineralizations (Geisler et al., 2007; Li et al., 2014; Soman et al., 2010). In the presence of a halogen-rich (F, Cl, Br, I) and fluids (H_2O), incompatible elements such as Hf, Th, U, Nb, Ta, Y, P, and Pb become highly mobile (Bau, 1996). Element mobilization is particularly active during fluid transition associated with metasomatic processes in mildly and highly evolved granites (Nardi et al., 2013; Yang et al., 2014). Several workers (Ogunleye et al., 2006) have shown that ore-bearing (Sn—W, Pb—Zn and Nb-REE) granites in the Nigerian younger granites are significantly enriched in fluorine (up to 6 wt%) compared to barren granite. Based on chemical compositions in zircon, vital magmatic to hydrothermal trends can be elucidated from several geochemical ratios (e.g., Y/Ho, Ce/Ce* and, Eu/Eu*). Although Y/Ho values are relatively stable during fractional crystallization of silicate melts, they are susceptible to late-stage magmatic and hydrothermal processes (Breiter et al., 2013). Y/Ho values for the unmineralized and mineralized samples (9.8–27) reflect late-stage evolution in the presence of a fluid phase (Breiter et al., 2009). Moreover, increased mobility of Y compared to Ho during hydrothermal regimes result in lower Y/Ho values in the Jigawa granites (Bau, 1996). Furthermore, Eu/Eu* and Ce/Ce* values in zircon provide a robust tool to track the reduced nature of magma during varying stage of zircon crystallization (Claiborne et al., 2010). Eu/Eu* in zircon is particularly sensitive to plagioclase fractionation and accumulation during evolution of the parental melt (Dunn and Sen, 1994). Mineralized biotite granites from the Nigerian Younger granite province typically contain plagioclase (Girei et al., 2020). Plagioclase is also present in the Jigawa granites. Therefore, we consider Eu/Eu* values as unreliable markers of redox conditions for the Jigawa Pb—Zn rich biotite granites. Variable Ce/Ce* values are associated with magmatic and hydrothermal zircon in the Jigawa Pb—Zn field (Supplementary Table 3). Average Ce/Ce* values from magmatic and hydrothermally altered zircon grains from the Jigawa Pb—Zn deposit ranges from 77.54 (22–152.98) in CHR1, 115.0 (99.40–276.95) & 7.4 (2.18–23.9) in KLK1A, 77.20 (1.80–214.0) & 12.7 (1.80–18.57) in ALT1A, 471 (64–1752) in sample AT1B, 361 (181–655) in sample JK1A and 433 (32–4426) in sample JK6A. Compared to the magmatic zircon, low Ce/Ce* values for hydrothermal zircon suggest that hydrothermal zircon formed under relatively reduced condition (Ballard et al., 2002; Pelleter et al., 2007).

5.5. Magmatic-metallogenetic model for the Jigawa Pb—Zn mineralization

Based on zircon U/Pb ages, geochemical signatures and zircon crystallization temperatures recorded from magmatic and hydrothermally altered zircon in the Koluki-Burra centre, a magmatic-hydrothermal model (Fig. 13) is proposed for the Jigawa Pb—Zn mineralization:

Stage 1: During stage 1 (192–190 Ma), emplacement of medium-coarse grained biotite granites took place (KLK1A, AT1A) in the Koluki-Burra centre. Zircons that crystalized during this stage display "100" prisms, with lower LREE, stronger Ce anomalies and Eu anomalies (Fig. 8b-c).

During stage 2, early stage metasomatism associated with the formation of barren quartz veins occurred, a process that was accompanied by silicification and potassic metasomatism (Fig. 3a-b).

During stage 3, later staged metasomatism marked by intense metamictization. Zircon dissolution-reprecipitation reactions during this lower temperature regime (550-650 °C) lead to the formation of hydrothermally altered zircons ("110" zircon grains) in the Jigawa biotite granites. This stage is marked by increased trace element concentration, fluid and mineral inclusion in these hydrothermally altered zircons (Supplementary Table 3; Fig. 5e; Fig. 8b-c). Deposition of ore-stage sulphides also took place during this stage.

Reactivation of transcurrent faults caused by changes in the direction of plate movement is proposed as the driving mechanism for magma intrusion and subsequent magmatic-hydrothermal episodes in the Ningi-Burra complex and elsewhere (Girei et al., 2019; Girei et al., 2020). Highly evolved granitic suites in the Nigerian Younger Granites are potential reservoirs for world-class mineralization. Moreover, almost all these evolved suites (usually biotite granites) in the Nigerian Younger Granite province show evidence for post-magmatic alterations (Girei et al., 2019; Ike, 1983; Kinnaird, 1985). This study has shown that zircon Zr/Hf, Y/Ho and Ce/Ce* values can be used to constrain the degree of evolution and oxidation in granites which provide useful clues for ore deposit exploration (Breiter et al., 2014; Loader et al., 2017).

6. Conclusions

1. Zircon U—Pb ages from unmineralized and mineralized suites from the Ningi-Burra anorogenic ring complex record complex magmatic and hydrothermal episodes associated with Pb—Zn mineralization. The main magmatic-hydrothermal episodes took place between 191 and 189 Ma.
2. Zircon Lu/Hf isotopes from the Ningi-Burra complex reflect magmatic origin from partial melting of the lower crustal with contributions from mantle-derived melts. Geochemical and Lu/Hf variations in magmatic and hydrothermal zircon constrain a common magmatic source for the zircon grains from the Jigawa Pb—Zn mineralization, but the differences in concentrations of trace elements and $^{176}Lu/^{177}Hf$ and $^{176}Yb/^{177}Hf$ ratios in the hydrothermal zircon grains can be attributed to higher mobility of the trace elements and Lu—Yb in the presence of a fluid phase.
3. Extensive fluid circulation caused leaching of metals from Pb-rich basement rocks and facilitated the formation of Zn—Pb mineralization in the Ningi-Burra complex.

Supplementary data to this article can be found online at https://doi.org/10.1016/j.lithos.2021.106115.

Declaration of Competing Interest

The authors declare that they have no known competing financial interests or personal relationships that could have appeared to influence the work reported in this paper.

Acknowledgements

This work was financed by the National Natural Science Foundation of China (Grant No. 41502067). We are grateful to two anonymous reviewers for their constructive comments and suggestions that significantly improved this study. We also thank Dr. Greg Shellnutt and Dr. Parthiban Rajendran for their editorial handling of this paper.

References

Abaa, S., 1991. Hydrothermal fluids responsible for the formation of precious minerals in the Nigerian Younger Granite Province. Mineral. Deposita 26, 34–39.
Amuda, A.K., Yang, X., Deng, J., Faisal, M., Cao, J., Bute, S.I., Girei, M.B., Elatikpo, S.M., 2020. Petrogenesis of the peralkaline Dutsen Wai and Ropp complexes in the Nigerian younger granites: implications for crucial metal enrichments. Int. Geol. Rev. 1–25.
Anderson, A.J., Wirth, R., Thomas, R., 2008. The alteration of metamict zircon and its role in the remobilization of high-field-strength elements in the Georgeville granite, Nova Scotia. Can. Mineral. 46, 1–18.
Ballard, J.R., Palin, M.J., Campbell, I.H., 2002. Relative oxidation states of magmas inferred from Ce (IV)/Ce (III) in zircon: application to porphyry copper deposits of northern Chile. Contrib. Mineral. Petrol. 144, 347–364.
Barth, A.P., Wooden, J.L., 2010. Coupled elemental and isotopic analyses of polygenetic zircons from granitic rocks by ion microprobe, with implications for melt evolution and the sources of granitic magmas. Chem. Geol. 277, 149–159.
Batchelor, R., Bowden, P., 1986. Major and trace element analyses of volcanic and subvolcanic igneous rocks from the Nigeria–Niger anorogenic province. Overseas Development Administration. Research Scheme 2679.
Bau, M., 1996. Controls on the fractionation of isovalent trace elements in magmatic and aqueous systems: evidence from Y/Ho, Zr/Hf, and lanthanide tetrad effect. Contrib. Mineral. Petrol. 123, 323–333.
Bell, E.A., Boehnke, P., Barboni, M., Harrison, T.M., 2019. Tracking chemical alteration in magmatic zircon using rare earth element abundances. Chem. Geol. 510, 56–71.
Belousova, E., Griffin, W.L., O'Reilly, S.Y., Fisher, N., 2002. Igneous zircon: trace element composition as an indicator of source rock type. Contrib. Mineral. Petrol. 143, 602–622.
Belousova, E., Griffin, W., O'REILLY, S.Y., 2006. Zircon crystal morphology, trace element signatures and Hf isotope composition as a tool for petrogenetic modelling: examples from Eastern Australian granitoids. J. Petrol. 47, 329–353.
Black, R., Caby, R., Moussine-Pouchkine, A., Bayer, R., Bertrand, J., Boullier, A., Fabre, J., Lesquer, A., 1979. Evidence for late Precambrian plate tectonics in West Africa. Nature 278, 223.
Black, R., Lameyre, J., Bonin, B., 1985. The structural setting of alkaline complexes. J. Afr. Earth Sci. 3, 5–16.
Bowden, P., Kinnaird, J., 1984. The petrology and geochemistry of alkaline granites from Nigeria. Phys. Earth Planet. Inter. 35, 199–211.
Breiter, K., Čopjaková, R., Škoda, R., 2009. The involvement of F, CO2, and As in the alteration of Zr–Th–REE-bearing accessory minerals in the Hora Svaté Kateriny A-type granite, Czech Republic. Can. Mineral. 47, 1375–1398.
Breiter, K., Gardenová, N., Kanický, V., Vaculovič, T., 2013. Gallium and germanium geochemistry during magmatic fractionation and post-magmatic alteration in different types of granitoids: a case study from the Bohemian Massif (Czech Republic). Geol. Carpathica 64, 171–180.
Breiter, K., Lamarão, C.N., Borges, R.M.K., Dall'Agnol, R., 2014. Chemical characteristics of zircon from A-type granites and comparison to zircon of S-type granites. Lithos 192, 208–225.
Bute, S.I., Yang, X., Cao, J., Liu, L., Deng, J., Haruna, I.V., Girei, M.B., Abubakar, U., Akhtar, S., 2019. Origin and Tectonic Implications of Ferroan Alkali-calcific Granitoids from the Hawal Massif, East-eastern Nigeria Terrane: Clues from Geochemistry and Zircon U-Pb-Hf Isotopes.
Castiñeiras, P., Navidad, M., Casas, J.M., Liesa, M., Carreras, J., 2011. Petrogenesis of Ordovician magmatism in the Pyrenees (Albera and Canigó Massifs) determined on the basis of zircon minor and trace element composition. J. Geol. 119, 521–534.
Claiborne, L.L., Miller, C., Walker, B., Wooden, J., Mazdab, F., Bea, F., 2006. Tracking magmatic processes through Zr/Hf ratios in rocks and Hf and Ti zoning in zircons: an example from the Spirit Mountain batholith, Nevada. Mineral. Mag. 70, 517–543.
Claiborne, L.L., Miller, C.F., Wooden, J.L., 2010. Trace element composition of igneous zircon: a thermal and compositional record of the accumulation and evolution of a large silicic batholith, Spirit Mountain, Nevada. Contrib. Mineral. Petrol. 160, 511–531.
Claoué, J., King, R., Kerrich, R., 1990. Archaean hydrothermal zircon in the Abitibi greenstone belt: constraints on the timing of gold mineralisation. Earth Planet. Sci. Lett. 98, 109–128.
Dickin, A., Halliday, A., Bowden, P., 1991. A Pb, Sr and Nd isotope study of the basement and Mesozoic ring complexes of the Jos Plateau, Nigeria. Chem. Geol. 94, 23–32.
du Bray, E.A., Bacon, C.R., John, D.A., Wooden, J.L., Mazdab, F.K., 2011. Episodic intrusion, internal differentiation, and hydrothermal alteration of the Miocene Tatoosh intrusive suite south of Mount Rainier, Washington. Bulletin 123, 534–561.
Dunn, T., Sen, C., 1994. Mineral/matrix partition coefficients for orthopyroxene, plagioclase, and olivine in basaltic to andesitic systems: a combined analytical and experimental study. Geochim. Cosmochim. Acta 58, 717–733.
Fu, B., Page, F.Z., Cavosie, A.J., Fournelle, J., Kita, N.T., Lackey, J.S., Wilde, S.A., Valley, J.W., 2008. Ti-in-zircon thermometry: applications and limitations. Contrib. Mineral. Petrol. 156, 197–215.

Geisler, T., Pidgeon, R.T., Kurtz, R., Van Bronswijk, W., Schleicher, H., 2003a. Experimental hydrothermal alteration of partially metamict zircon. Am. Mineral. 88, 1496–1513.
Geisler, T., Rashwan, A., Rahn, M., Poller, U., Zwingmann, H., Pidgeon, R., Schleicher, H., Tomaschek, F., 2003b. Low-temperature hydrothermal alteration of natural metamict zircons from the Eastern Desert, Egypt. Mineral. Mag. 67, 485–508.
Geisler, T., Schaltegger, U., Tomaschek, F., 2007. Re-equilibration of zircon in aqueous fluids and melts. Elements 3, 43–50.
Girei, M.B., Li, H., Algeo, T.J., Bonin, B., Ogunleye, P.O., Bute, S.I., Ahmed, H.A., 2019. Petrogenesis of A-type granites associated with Sn–Nb–Zn mineralization in Ririwai complex, north-Central Nigeria: constraints from whole-rock SmNd and zircon LuHf isotope systematics. Lithos 340, 49–70.
Girei, M.B., Li, H., Vincent, V.I., Algeo, T.J., Elatikpo, S.M., Bute, S.I., Ahmed, H.A., Amuda, A.K., 2020. Genesis and timing of Mo mineralization in the Mada Ring Complex, north-central Nigeria: insights from whole-rock geochemistry, Nd-Sr isotopes, zircon U-Pb-Hf isotopes, and molybdenite Re-Os systematics. Mineral. Deposita 1–20.
Griffin, W., Wang, X., Jackson, S., Pearson, N., O'Reilly, S.Y., Xu, X., Zhou, X., 2002. Zircon chemistry and magma mixing, SE China: in-situ analysis of Hf isotopes, Tonglu and Pingtan igneous complexes. Lithos 61, 237–269.
Grimes, C.B., John, B.E., Cheadle, M.J., Mazdab, F.K., Wooden, J.L., Swapp, S., Schwartz, J.J., 2009. On the occurrence, trace element geochemistry, and crystallization history of zircon from in situ ocean lithosphere. Contrib. Mineral. Petrol. 158, 757.
Grimes, C., Wooden, J., Cheadle, M., John, B., 2015. "Fingerprinting" tectono-magmatic provenance using trace elements in igneous zircon. Contrib. Mineral. Petrol. 170, 46.
Harlov, D., Lewerentz, A., Schersten, A., 2012. Alteration of zircon in alkaline fluids: nature and experiment. Mineral. Mag. 76, 1813.
Harrison, T.M., Schmitt, A.K., 2007. High sensitivity mapping of Ti distributions in Hadean zircons. Earth Planet. Sci. Lett. 261, 9–19.
Hayashi, M., Shinno, I., 1990. Morphology of synthetic zircon crystals doped with various elements. Mineral. J. 15, 119–128.
Hoskin, P.W., 2005. Trace-element composition of hydrothermal zircon and the alteration of Hadean zircon from the Jack Hills, Australia. Geochim. Cosmochim. Acta 69, 637–648.
Hoskin, P.W., Schaltegger, U., 2003. The composition of zircon and igneous and metamorphic petrogenesis. Rev. Mineral. Geochem. 53, 27–62.
Hu, Z., Liu, Y., Gao, S., Liu, W., Zhang, W., Tong, X., Lin, L., Zong, K., Li, M., Chen, H., 2012. Improved in situ Hf isotope ratio analysis of zircon using newly designed X skimmer cone and jet sample cone in combination with the addition of nitrogen by laser ablation multiple collector ICP-MS. J. Anal. At. Spectrom. 27, 1391–1399.
Ike, E., 1983. The structural evolution of the Tibchi ring-complex: a case study for the Nigerian Younger Granite Province. J. Geol. Soc. 140, 781–788.
Jiang, W.-C., Li, H., Evans, N.J., Wu, J.-H., 2019a. Zircon records multiple magmatic-hydrothermal processes at the giant Shizhuyuan W–Sn–Mo–Bi polymetallic deposit, South China. Ore Geol. Rev. 115, 103160.
Jiang, W.-C., Li, H., Mathur, R., Wu, J.-H., 2019b. Genesis of the giant Shizhuyuan W–Sn–Mo–Bi–Pb–Zn polymetallic deposit, South China: constraints from zircon geochronology and geochemistry in skarns. Ore Geol. Rev. 102980.
Kamaunji, V.D., Wang, L.-X., Ahmed, H.A., Zhu, Y.-X., Vincent, V.I., Girei, M.B., 2020. Coexisting A 1 and A 2 granites of Kudaru Complex: implications for genetic and tectonic diversity of A-type granite in the Younger Granite province, north-central Nigeria. Int. J. Earth Sci. 109, 511–535.
Kebede, T., Horie, K., Hidaka, H., Terada, K., 2007. Zircon 'microvein'in peralkaline granitic gneiss, western Ethiopia: origin, SHRIMP U–Pb geochronology and trace element investigations. Chem. Geol. 242, 76–102.
Kemp, A., Hawkesworth, C., Paterson, B., Kinny, P., 2006. Episodic growth of the Gondwana supercontinent from hafnium and oxygen isotopes in zircon. Nature 439, 580–583.
Kemp, A., Hawkesworth, C., Foster, G., Paterson, B., Woodhead, J., Hergt, J., Gray, C., Whitehouse, M., 2007. Magmatic and crustal differentiation history of granitic rocks from Hf-O isotopes in zircon. Science 315, 980–983.
Kinnaird, J., 1984. Contrasting styles of Sn-Nb-Ta-Zn mineralization in Nigeria. J. Afr. Earth Sci. 2, 81–90.
Kinnaird, J., 1985. Hydrothermal alteration and mineralization of the alkaline anorogenic ring complexes of Nigeria. J. Afr. Earth Sci. 3, 229–251.
Kinnaird, J., Bowden, P., Ixer, R., Odling, N., 1985. Mineralogy, geochemistry and mineralization of the Ririwai complex, northern Nigeria. J. Afr. Earth Sci. 3, 185–222.
Klötzli, U., Klötzli, E., Günes, Z., Kosler, J., 2009. Accuracy of laser ablation U-Pb zircon dating: results from a test using five different reference zircons. Geostand. Geoanal. Res. 33, 5–15.
Lewerentz, A., Harlov, D.E., Scherstén, A., Whitehouse, M.J., 2019. Baddeleyite formation in zircon by Ca-bearing fluids in silica-saturated systems in nature and experiment: resetting of the U–Pb geochronometer. Contrib. Mineral. Petrol. 174, 64.
Li, H., Watanabe, K., Yonezu, K., 2014. Zircon morphology, geochronology and trace element geochemistry of the granites from the Huangshaping polymetallic deposit, South China: implications for the magmatic evolution and mineralization processes. Ore Geol. Rev. 60, 14–35.
Li, H., Wu, J.-H., Evans, N.J., Jiang, W.-C., Zhou, Z.-K., 2018. Zircon geochronology and geochemistry of the Xianghualing A-type granitic rocks: insights into multi-stage Sn-polymetallic mineralization in South China. Lithos 312, 1–20.
Linnen, R.L., Keppler, H., 2002. Melt composition control of Zr/Hf fractionation in magmatic processes. Geochim. Cosmochim. Acta 66, 3293–3301.
Liu, Y., Hu, Z., Gao, S., Günther, D., Xu, J., Gao, C., Chen, H., 2008. In situ analysis of major and trace elements of anhydrous minerals by LA-ICP-MS without applying an internal standard. Chem. Geol. 257, 34–43.
Loader, M.A., Wilkinson, J.J., Armstrong, R.N., 2017. The effect of titanite crystallisation on Eu and Ce anomalies in zircon and its implications for the assessment of porphyry Cu deposit fertility. Earth Planet. Sci. Lett. 472, 107–119.
Ludwig, K.R., 2003. User's manual for isoplot 3.00, a geochronlogical toolkit for microsoft excel. Berkeley Geochronl. Cent. Spec. Publ. 4, 25–32.
Machado, N., Simonetti, A., 2001. U-Pb dating and Hf isotopic composition of zircon by laser-ablation-MC-ICP-MS. Laser Ablation-ICPMS in the Earth Sciences: Principles and Applications. 29, pp. 121–146.
Nardi, L., Formoso, M., Müller, I., Fontana, E., Jarvis, K., Lamarão, C., 2013. Zircon/rock partition coefficients of REEs, Y, Th, U, Nb, and Ta in granitic rocks: Uses for provenance and mineral exploration purposes. Chem. Geol. 335, 1–7.
Ogunleye, P., Garba, I., Ike, E., 2006. Factors contributing to enrichment and crystallization of niobium in pyrochlore in the Kaffo albite arfvedsonite granite, Ririwai Complex, Younger Granites province of Nigeria. J. Afr. Earth Sci. 44, 372–382.
Olatunji, J., Ekwere, S., 1986. Alteration and base metal sulfide mineralization in the porphyries of the Banke Complex, Northern Nigeria. Econ. Geol. 81, 984–989.
Pearce, J.A., Harris, N.B., Tindle, A.G., 1984. Trace element discrimination diagrams for the tectonic interpretation of granitic rocks. J. Petrol. 25, 956–983.
Pelleter, E., Cheilletz, A., Gasquet, D., Mouttaqi, A., Annich, M., El Hakour, A., Deloule, E., Féraud, G., 2007. Hydrothermal zircons: a tool for ion microprobe U–Pb dating of gold mineralization (Tamlalt–Menhouhou gold deposit—Morocco). Chem. Geol. 245, 135–161.
Pupin, J., 1980. Zircon and granite petrology. Contrib. Mineral. Petrol. 73, 207–220.
Rahaman, M., Van Breemen, O., Bowden, P., Bennett, J., 1984. Age migrations of anorogenic ring complexes in Northern Nigeria. J. Geol. 92, 173–184.
Rubin, J.N., Henry, C.D., Price, J.G., 1993. The mobility of zirconium and other "immobile" elements during hydrothermal alteration. Chem. Geol. 110, 29–47.
Schiller, D., Finger, F., 2019. Application of Ti-in-zircon thermometry to granite studies: problems and possible solutions. Contrib. Mineral. Petrol. 174, 51.
Schoene, B., Latkoczy, C., Schaltegger, U., Günther, D., 2010. A new method integrating high-precision U–Pb geochronology with zircon trace element analysis (U–Pb TIMS-TEA). Geochim. Cosmochim. Acta 74, 7144–7159.
Sheard, E.R., Williams-Jones, A.E., Heiligmann, M., Pederson, C., Trueman, D.L., 2012. Controls on the concentration of zirconium, niobium, and the rare earth elements in the Thor Lake rare metal deposit, Northwest Territories, Canada. Econ. Geol. 107, 81–104.
Soman, A., Geisler, T., Tomaschek, F., Grange, M., Berndt, J., 2010. Alteration of crystalline zircon solid solutions: a case study on zircon from an alkaline pegmatite from Zomba–Malosa, Malawi. Contrib. Mineral. Petrol. 160, 909–930.
Thompson, P.M., Kempton, P.D., Kerr, A.C., 2008. Evaluation of the effects of alteration and leaching on Sm–Nd and Lu–Hf systematics in submarine mafic rocks. Lithos 104, 164–176.
Turner, D., 1983. Upper Proterozoic schist belts in the Nigerian sector of the Pan-African Province of West Africa. Precambrian Res. 21, 55–79.
Turner, D., Bowden, P., 1979. The Ningi-Burra complex, Nigeria: dissected calderas and migrating magmatic centres. J. Geol. Soc. 136, 105–119.
Valley, P.M., Fisher, C.M., Hanchar, J.M., Lam, R., Tubrett, M., 2010. Hafnium isotopes in zircon: a tracer of fluid-rock interaction during magnetite–apatite ("Kiruna-type") mineralization. Chem. Geol. 275, 208–220.
Wang, T.-G., Li, H., Liu, J.-S., Evans, N.J., Wang, Y.-C., Zha, D., 2019. Whole-rock and zircon geochemistry of the Xiaoliugou granites, North Qilian Orogen (NW China): Implications for tectonic setting, magma evolution and W–Mo mineralization. Ore Geol. Rev. 115, 103166.
Watson, E.B., Harrison, T., 2005. Zircon thermometer reveals minimum melting conditions on earliest Earth. Science 308, 841–844.
Woodhead, J., Hergt, J., Shelley, M., Eggins, S., Kemp, R., 2004. Zircon Hf-isotope analysis with an excimer laser, depth profiling, ablation of complex geometries, and concomitant age estimation. Chem. Geol. 209, 121–135.
Yang, W.-B., Niu, H.-C., Shan, Q., Sun, W.-D., Zhang, H., Li, N.-B., Jiang, Y.-H., Yu, X.-Y., 2014. Geochemistry of magmatic and hydrothermal zircon from the highly evolved Baerzhe alkaline granite: implications for Zr–REE–Nb mineralization. Mineral. Deposita 49, 451–470.
Yuan, H.-L., Gao, S., Dai, M.-N., Zong, C.-L., Günther, D., Fontaine, G.H., Liu, X.-M., Diwu, C., 2008. Simultaneous determinations of U–Pb age, Hf isotopes and trace element compositions of zircon by excimer laser-ablation quadrupole and multiple-collector ICP-MS. Chem. Geol. 247, 100–118.
Zhu, J., Peng, S., Peng, L., 2016. U–Pb Dating of Hydrothermal Zircons from the Neoproterozoic Liushanyan VMS Cu–Zn Deposit, Central China: evidence for a Triassic Deformation Event. Resour. Geol. 66, 227–239.